

AD A045408

*[Handwritten signature]*

*12*

RADC-TR-77-288  
Final Technical Report  
August 1977



INFRARED RADIATION IN A REAL TROPICAL ATMOSPHERE  
AVCO Everett Research Laboratory, Inc.

Sponsored by  
Defense Advanced Research Projects Agency (DoD)  
ARPA Order No. 2837

DDC  
OCT 19 1977  
R

Approved for public release; distribution unlimited.

The views and conclusions contained in this document are those of the authors and should not be interpreted as necessarily representing the official policies, either expressed or implied, of the Defense Advanced Research Projects Agency or the U. S. Government.

AD No. \_\_\_\_\_  
DDC FILE COPY

ROME AIR DEVELOPMENT CENTER  
Air Force Systems Command  
Griffiss Air Force Base, New York 13441

This report has been reviewed by the RALC Information Office (OI) and is releasable to the National Technical Information Service (NTIS). At NTIS it will be releasable to the general public, including foreign nations.

This report has been reviewed and is approved for publication.

APPROVED:

*Homer L. Harkleroad Jr.*

Homer L. Harkleroad Jr., Captain, USAF  
Project Engineer

Do not return this copy. Retain or destroy.

UNCLASSIFIED

SECURITY CLASSIFICATION OF THIS PAGE (When Data Entered)

REPORT DOCUMENTATION PAGE		READ INSTRUCTIONS BEFORE COMPLETING FORM
1. REPORT NUMBER RADC-TR-77-288	2. GOVT ACCESSION NO.	3. RECIPIENT'S CATALOG NUMBER
4. TITLE (and Subtitle) INFRARED RADIATION IN A REAL TROPICAL ATMOSPHERE.	5. TYPE OF REPORT & PERIOD COVERED Final Technical Report, 1 Nov 75 - 30 Apr 77.	
7. AUTHOR(s) Lee A. Young	6. PERFORMING ORG. REPORT NUMBER N/A	
9. PERFORMING ORGANIZATION NAME AND ADDRESS AVCO Everett Research Laboratory, Inc. 2385 Revere Beach Parkway Everett MA 02149	8. CONTRACT OR GRANT NUMBER(s) F04701-75-C-0047 ARPA Order-2837	
11. CONTROLLING OFFICE NAME AND ADDRESS Defense Advanced Research Projects Agency 1400 Wilson Blvd Arlington VA 22209	10. PROGRAM ELEMENT PROJECT, TASK AREA & WORK UNIT NUMBERS 62301E 28370101	
14. MONITORING AGENCY NAME & ADDRESS (if different from Controlling Office) Rome Air Development Center (OCSE) Griffiss AFB NY 13441	12. REPORT DATE August 1977	
	13. NUMBER OF PAGES 90	
	15. SECURITY CLASS. (of this report) UNCLAS	
	15a. DECLASSIFICATION/DOWNGRADING SCHEDULE N/A	
16. DISTRIBUTION STATEMENT (of this Report) Approved for public release; distribution unlimited.		
17. DISTRIBUTION STATEMENT (of the abstract entered in Block 20, if different from Report) Same		
18. SUPPLEMENTARY NOTES RADC Project Engineer: Captain Homer L. Harkleroad Jr., (OCSE)		
19. KEY WORDS (Continue on reverse side if necessary and identify by block number) Infrared radiation    Curtis-Godson approximation    Radiosonde data Spectroscopy    Effective parameters    Trade-wind inversion AFGL compendium    Continuum radiation    Humidity Molecular absorption    Hawaiian Islands    Temporal fluctuations Water vapor    Tropical meteorology		
20. ABSTRACT (Continue on reverse side if necessary and identify by block number) Transmission of infrared radiation in the 8-13 and 16.5-21 $\mu$ m spectral regions from 3 km altitude through the atmosphere to outer space has been evaluated. Analysis of tropical radiosonde atmospheric profiles of temperature and humidity shows that fluctuations in the total amount of water vapor above 3 km cause the transmission to vary by amounts from 10% to two orders of magnitude. Fluctuations in the effective temperature or pressure for absorption are shown to be small. The Curtis-Godson approximation is analyzed in detail for this problem. Also, effective parameters describing an atmospheric slant path		

DD FORM 1 JAN 73 1473 EDITION OF 1 NOV 65 IS OBSOLETE

UNCLASSIFIED

SECURITY CLASSIFICATION OF THIS PAGE (When Data Entered)

048450

next page

LB


UNCLASSIFIED

SECURITY CLASSIFICATION OF THIS PAGE(When Data Entered)

are formulated for absorption by the water vapor continuum.

The total amount of water vapor above 3 km varies chiefly as the trade wind inversion rises above or falls below that altitude; it correlates poorly with the absolute humidity at 3 km.

The atmospheric transmission can be obtained in real time from measurements of atmospheric emission. Fluctuations in the effective emission temperature, calculated from radiosonde data, are relatively small. However, further study of the effect of cirrus clouds on the transmission-emission relationship would be desirable.



UNCLASSIFIED

SECURITY CLASSIFICATION OF THIS PAGE(When Data Entered)

INFRARED RADIATION IN A REAL TROPICAL ATMOSPHERE

Lee A. Young

Contractor: AVCO Everett Research Laboratory, Inc.  
Contract Number: F04701-75-C-0047  
Effective Date of Contract: 1 November 1974  
Contract Expiration Date: 31 December 1977  
Short Title of Work: Infrared Radiation in a Real  
Tropical Atmosphere  
Program Code Number: 5E20  
Period of Work Covered: Nov 75 - Apr 77

Principal Investigator: Dr. Lee A. Young  
Phone: 617 389-3000, Ext 615  
Project Engineer: Captain Homer L. Harkleroad Jr.  
Phone: 315 330-3144

Approved for public release;  
distribution unlimited.

This research was supported by the Defense Advanced  
Research Projects Agency of the Department of  
Defense and was monitored by Captain Homer L. Harkleroad Jr.  
(OCSE), Griffiss AFB NY 13441 under Contract  
F04701-75-C-0047.

ACCESSION for	
NTIS	White Section <input checked="" type="checkbox"/>
DDC	Buff Section <input type="checkbox"/>
UNANNOUNCED DISSEMINATION	<input type="checkbox"/>
BY	
DISTRIBUTION/AVAILABILITY CODES	
SPECIAL	
A	

## ABSTRACT

Transmission of infrared radiation in the 8-13 and 16.5-21  $\mu\text{m}$  spectral regions from 3 km altitude through the atmosphere to outer space has been evaluated. Analysis of tropical radiosonde atmospheric profiles of temperature and humidity shows that fluctuations in the total amount of water vapor above 3 km cause the transmission to vary by amounts from 10% to two orders of magnitude. Fluctuations in the effective temperature or pressure for absorption are shown to be small. The Curtis-Godson approximation is analyzed in detail for this problem. Also, effective parameters describing an atmospheric slant path are formulated for absorption by the water vapor continuum.

The total amount of water vapor above 3 km varies chiefly as the trade wind inversion rises above or falls below that altitude; it correlates poorly with the absolute humidity at 3 km.

The atmospheric transmission can be obtained in real time from measurements of atmospheric emission. Fluctuations in the effective emission temperature, calculated from radiosonde data, are relatively small. However, further study of the effect of cirrus clouds on the transmission-emission relationship would be desirable.

## TABLE OF CONTENTS

<u>Section</u>		<u>Page</u>
	Foreword	ii
	Abstract	iii
	List of Illustrations	vii
1.0	INTRODUCTION AND SUMMARY	1
2.0	ATMOSPHERIC ABSORPTION - THEORY	5
	2.1 Curtis-Godson Approximation	5
	2.2 Accuracy of C. -G. Approximation in an Exponential, Mixed, Isothermal Model Atmosphere	12
	2.2.1 Curtis-Godson Approximation	12
	2.2.2 Exact	14
	2.3 C. -G. Approximation Applied to Exponentially Mixed, Isothermal Atmosphere	18
	2.4 C. -G Approximation Applied to Exponentially Mixed Atmosphere with Linear Temperature Variation	21
	2.5 Effective Parameters for the Water Vapor Continuum	24
3.0	ATMOSPHERIC EMISSION - THEORY	29
	3.1 Line Emission	29
	3.2 Band Emission	32
4.0	ABSORPTION AND EMISSION PARAMETERS FOR A REAL TROPICAL ATMOSPHERE	35
	4.1 Tropical Meteorology	35
	4.2 Atmospheric Radiosonde Data	41
	4.3 Curtis-Godson Parameters for Absorption in Hawaiian Islands Atmospheres	42
	4.4 Relevance of Hilo Data to Mt. Haleakala	50
	4.5 Emission Parameters for Hawaiian Islands Atmosphere	51

<u>Section</u>		<u>Page</u>
5.0	ABSORPTION PREDICTIONS	59
	5.1 Spectroscopic Parameters	59
	5.2 Transmission in 16-21 $\mu\text{m}$ Window	63
	5.3 Transmission in the 8-13 $\mu\text{m}$ Window	70
6.0	CONCLUSIONS	79
	Acknowledgement	87
	References	89



## LIST OF ILLUSTRATIONS

<u>Figure</u>		<u>Page</u>
1	Average Absorption, Emissivity and Transmission of a Spectral Band	7
2	Curve of Growth for a Lorentz (Collision-Broadened) Spectral Line	9
3	Equivalent Linewidth in Exponential Atmosphere	16
4	Error of Curtis-Godson Approximation	17
5	Humidity Profiles Derived from Rawinsonde Data for Hilo, Hawaii at Midnight GMT (July)	37
6	Humidity Profiles for Hilo at Noon GMT (July)	38
7	Temperature Profiles for Hilo at Noon GMT (July)	39
8	Humidity Profiles for Hilo at Noon GMT (January)	40
9	Amount of Water Vapor Above 3 km for Hilo at Midnight GMT (1970-71)	43
10	Amount of Water Vapor Above 3 km for Hilo at Noon GMT (1970-71)	44
11	Total Amount of Water Vapor Above 3 km vs Absolute Humidity at 3 km for Hilo (Summer)	45
12	Total Amount of Water Vapor Above 3 km vs Absolute Humidity at 3 km for Hilo (Winter)	46
13	History of Effective Line Strength (S) and Width ( $\gamma$ ) Above 3 km for Hilo at Midnight GMT (1970-71)	47
14	History of Effective Line Strength (S) and Width ( $\gamma$ ) Above 3 km for Hilo at Noon GMT (1970-71)	48
15	Effective Blackbody Spectral Radiance for Atmospheric Line Emission at 3 km Above Hilo	52
16	Effective Blackbody Temperature for Atmospheric Line Radiation, as seen from 3 km Above Hilo	53

<u>Figure</u>		<u>Page</u>
17	Effective Blackbody Spectral Radiance for Atmospheric Band Radiation at 3 km Above Hilo	55
18	Effective Blackbody Temperature for Atmospheric Band Radiation, as seen from 3 km Above Hilo	56
19	Spectral Band Radiance of Atmospheric Water Vapor Above 3 km at Hilo	58
20	Transmission by Water Vapor Over 600 ft Path (20-25 $\mu$ )	61
21	Transmission by Water Vapor Over 600 ft Path (15.2-20 $\mu$ )	62
22	Transmission Through a Humid Tropical Atmosphere	64
23	Transmission by H <sub>2</sub> O Lines and Continuum in 16-21 $\mu$ Window vs u	65
24	Map of Transmission by H <sub>2</sub> O Lines in 16-21 $\mu$ m Band	67
25	Map of Transmission by H <sub>2</sub> O Continuum in 16-21 $\mu$ m Band	68
26	Transmission by CO <sub>2</sub> Lines vs Elevation Angle in 16-21 $\mu$ m Band	69
27	Transmission by H <sub>2</sub> O Lines in 8-13 $\mu$ m Band vs u	71
28	Map of Transmission by H <sub>2</sub> O Lines in 8-13 $\mu$ m Band	72
29	Transmission by H <sub>2</sub> O Continuum in 8-13 $\mu$ m Band vs u	73
30	Transmission by H <sub>2</sub> O Continuum 8-13 $\mu$ m Band vs u <sup>2</sup> /l	74
31	Map of Transmission by H <sub>2</sub> O Continuum in the 8-13 $\mu$ m Band	75
32	Transmission by CO <sub>2</sub> and O <sub>3</sub> in the 8-13 $\mu$ m Band	77
33	Predicted Transmission from 3 km to Outer Space vs Elevation Angle	80
34	Predicted Transmission from 3 km to Outer Space vs Elevation Angle	81
35	Emissivity of the Sky Measured by H. Kent at AMOS, for Various Assumed Atmospheric Temperatures	83
36	Emissivity of the Sky Measured by H. Kent at AMOS, for Various Assumed Atmospheric Temperatures	84

## 1.0 INTRODUCTION AND SUMMARY

Quantitative interpretation of infrared measurements through the atmosphere requires accurate specification of atmospheric absorption. Convenient yet accurate models of radiative transfer are needed, as well as knowledge of the concentration of atmospheric absorbers. Among the latter, water vapor is notable for its spatial and temporal variability.

For the past three and one-half years a multichannel infrared telescope\* located at an altitude of 3.0 km on the summit of Mt. Haleakala on the island of Maui in the Hawaiian Islands has been used to study extra-atmospheric sources. This instrument is mounted on a 1.2 m telescope and has two spectral channels which are particularly useful for measurements on objects of low color temperature: No. 5 at 8.3 to 13.4  $\mu\text{m}$  and No. 6 at 16.5 to 20.8  $\mu\text{m}$ . The site lies above most aerosols and cumulus clouds. Nevertheless, atmospheric absorption is significant in Channel 6 at all times and in Channel 5 under humid conditions or at low elevation angles.

In this report we show that the fluctuations in the amount of water vapor above 3 km in tropical atmospheres are sufficient to make reference to typical or model conditions of little value. We explore the feasibility of obtaining real-time information on atmospheric transmission from sky emission measurements. This procedure is favored by our demonstration

---

\*The instrument is known as the Advanced Multi-Color Tracker for AMOS (AMTA), and is a facility of the ARPA-Maui Optical Station (AMOS), which is operated under the direction of the Avco Everett Research Laboratory, Inc.

that the effective temperature of the atmosphere for molecular emission is independent of elevation angle and has small temporal fluctuations. However, there are some discrepancies between our theoretical results and field measurements of sky brightness which deserve further investigation, with attention to the optical effects of thin cirrus clouds.

This work includes careful formulation of effective parameters for determination of the absorption or emission along a slant path through the atmosphere. Local radiosonde atmospheric profiles are utilized to display the temporal fluctuations of these parameters.

In Section 2.0 we show that the extinction properties of an atmospheric slant path for molecular band absorption can be specified with an accuracy of a few percent by three integral parameters. These are the optical depth and the effective strength and width of spectral lines. The latter two parameters are weighted averages along the path. Effective parameters for the water vapor continuum are also developed as weighted averages.

The theory of emission from molecular constituents in the atmosphere is presented in Section 3.0, with emphasis on the calculation of the effective atmospheric temperature.

In Section 4.0 we discuss tropical meteorology, and display profiles of water vapor concentration and temperature obtained from radiosonde data for the Hawaiian Islands. The history of the effective atmospheric parameters calculated from these tapes is displayed for a period of one year. The amount of water vapor above an altitude of 3 km is shown to fluctuate by a factor of 50, primarily because of variations of the altitude of the trade wind inversion or because of passage of large-scale cyclonic disturbances during the winter

months. The amount of water vapor above 3 km is poorly correlated with the local water vapor concentration at 3 km. On the other hand, the effective strengths and widths of absorbing spectral lines show very little temporal fluctuation. Also, the effective temperature for atmospheric emission varies relatively little over the course of a year. Consequently, all atmospheric properties which determine molecular absorption or emission above 3 km may be predicted with reasonable accuracy in advance except for the amount of water vapor overhead.

Predictions of atmospheric transmission in the 8-13 and 16.5-21  $\mu\text{m}$  spectral intervals are presented in Section 5.0, with elevation angle and amount of water vapor above 3 km as parameters. The effective width of each spectral line is calculated, using the AFCRL digital compilation of spectral line parameters. The transmission averaged over several lines is then obtained from appropriate band models. This scheme yields values of transmission by water vapor which are somewhat higher than laboratory measurements at Johns Hopkins, although the spectral shapes fit well. In the 16.5-21  $\mu\text{m}$  spectral region, water vapor is the most significant absorber. For low elevations and/or conditions of high humidity, the  $\text{H}_2\text{O}$  continuum (with foreign gas effects dominant) absorbs more than the individual lines. Transmission predictions based upon "average" conditions may be in error by as much as an order of magnitude. The 8-13  $\mu\text{m}$  window is much more transparent. Under dry conditions, the major absorber here is ozone, whose effect is predictable with relative confidence. For humid conditions the  $\text{H}_2\text{O}$  continuum becomes important. As the water vapor concentration increases, there is a transition from foreign gas effect domination to self "broadening".

The overall transmission by all absorbing species is presented in Section 6. The dependence of transmission on elevation angle is consistent with results from the single-parameter LOWTRAN 3 code, although the latter overestimates the transmission in the 16.5-21  $\mu\text{m}$  region by as much as an order of magnitude. Some discrepancies are found between our transmission predictions and estimates based upon atmospheric emission measurements. Further analysis of the relationship between these two should include use of radiosonde humidity profiles for the night of the emission measurements. Also, the emission, absorption and scattering by cirrus clouds should be addressed. That these effects may be significant is suggested by comparison of predicted and measured sky radiance.

## 2.0 ATMOSPHERIC ABSORPTION - THEORY

### 2.1 CURTIS-GODSON APPROXIMATION

We will show that to calculate the spectral absorption along a line of sight through the atmosphere it is not necessary to perform a spatial integral for each of the wavelengths of interest. Rather, the atmospheric path may be accurately represented by only three integral parameters which relate to (1) the total amount of absorbing species, (2) the effective average temperature along the path, and (3) the effective average pressure.

This approximation applies to isolated spectral lines or to a band of overlapping lines. (For continuum absorption, see Section 2.5.) Each line may be conveniently represented by its equivalent width, defined by

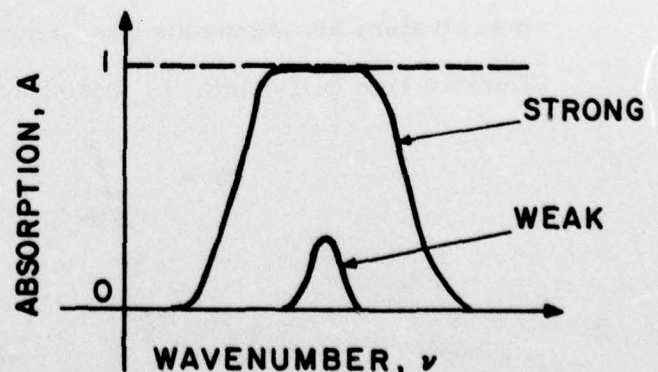
$$W = \int_{\text{line}} A(\nu) d\nu. \quad (1)$$

Here  $A(\nu)$  is the spectral absorptance profile of the line, seen at high spectral resolution. It is shown in the sketch below and is given by

$$A(\nu) = 1 - \exp - \int_{\text{path}} k(\nu) n d\ell. \quad (2)$$

The absorption coefficient,  $k(\nu)$ , and the concentration of absorbing species,  $n$ , vary along the path with distance  $\ell$ .

For a band of lines, the spectral absorption averaged over a region  $\Delta\nu$  containing many lines is of interest:



$$\bar{A} = 1 - \exp - \int_{\text{path}} \sum_i k_i(\nu) n dl \quad (3)$$

The summation is over all lines which contribute to absorption in  $\Delta\nu$ .

If the lines are weak with any spectral arrangement, or are strong and arranged at random on the spectral scale (statistical model), the average absorption is given by

$$\bar{A} = 1 - \exp - \bar{W}/\bar{d}, \quad (4)$$

where  $\bar{W}$  and  $\bar{d}$  are the average equivalent width and average spectral spacing within  $\Delta\nu$ . If the lines are strong, of the same strength, and regularly spaced (Elsasser model), we have

$$\bar{A} = \operatorname{erf}\left(\frac{\pi^{1/2}}{2}\right) \frac{W}{d} \quad (5)$$

These relations are plotted in Figure 1.

Combining Eqs. (1) and (2) for a Lorentz profile, we obtain

$$W = \int_{\text{line}} \left\{ 1 - \exp - \int_{\text{path}} \frac{1}{\pi} \frac{S \gamma du}{(\nu - \nu_0)^2 + \gamma^2} \right\} d\nu \quad (6)$$

(exact)

Here  $S = \int k(\nu) d\nu$  is the integrated absorption coefficient ("strength") of the line,  $\gamma$  is its half-width at half maximum, and  $\nu_0$  is the wavenumber at its center.

The Curtis-Godson approximation describes the absorbing path by an equivalent homogeneous gas sample having effective line strength  $\tilde{S}$ , effective line half-width  $\tilde{\gamma}$ , and optical depth

$$u = \int_{\text{path}} du = \int_{\text{path}} n dl \quad (7)$$



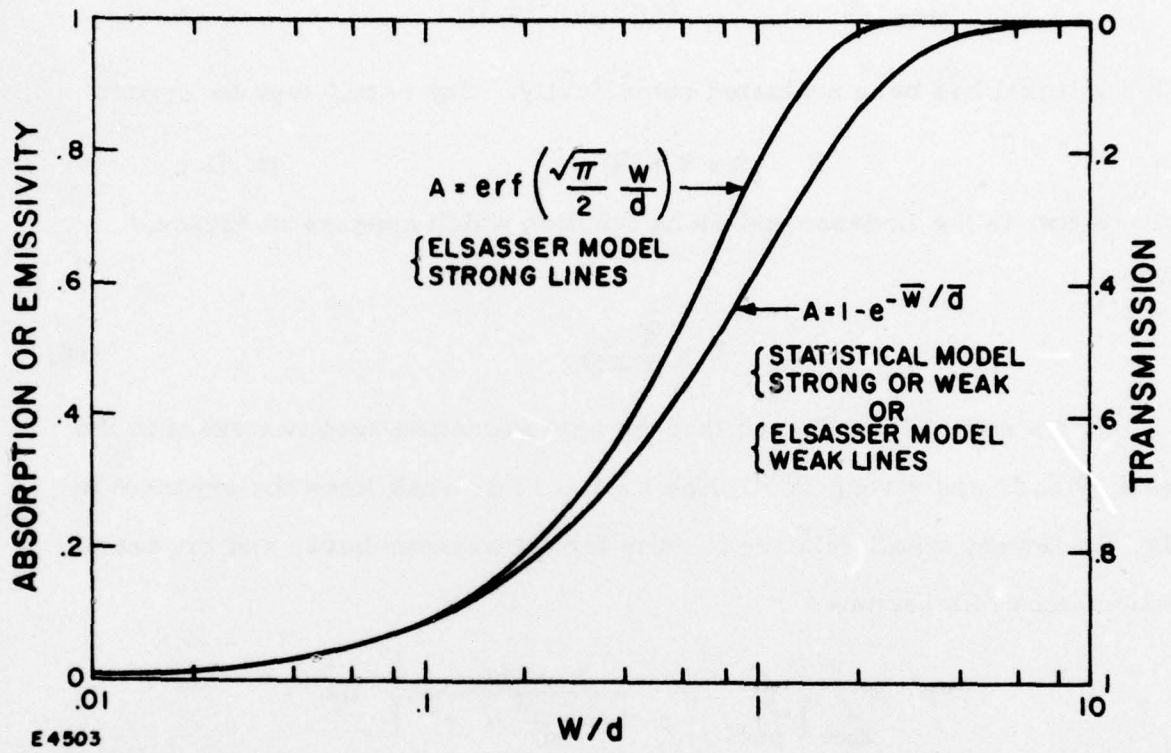


Figure 1. Average Absorption, Emissivity and Transmission of a Spectral Band

For such a sample Eq. (6) becomes

$$W = \int_{\text{line}} \left\{ 1 - \exp \frac{1}{\pi} \frac{\tilde{S} \tilde{\gamma} u}{(\nu - \nu_0)^2 + \tilde{\gamma}^2} \right\} d\nu \quad (\text{C.G.}) \quad (8)$$

This integral has been evaluated numerically. The result may be written

$$W = 2 \pi \tilde{\gamma} f(\tilde{x}) \quad (\text{C.G.}) \quad (9)$$

where  $f(x)$  is the Ladenburg-Reiche function which appears in Figure 2,

and

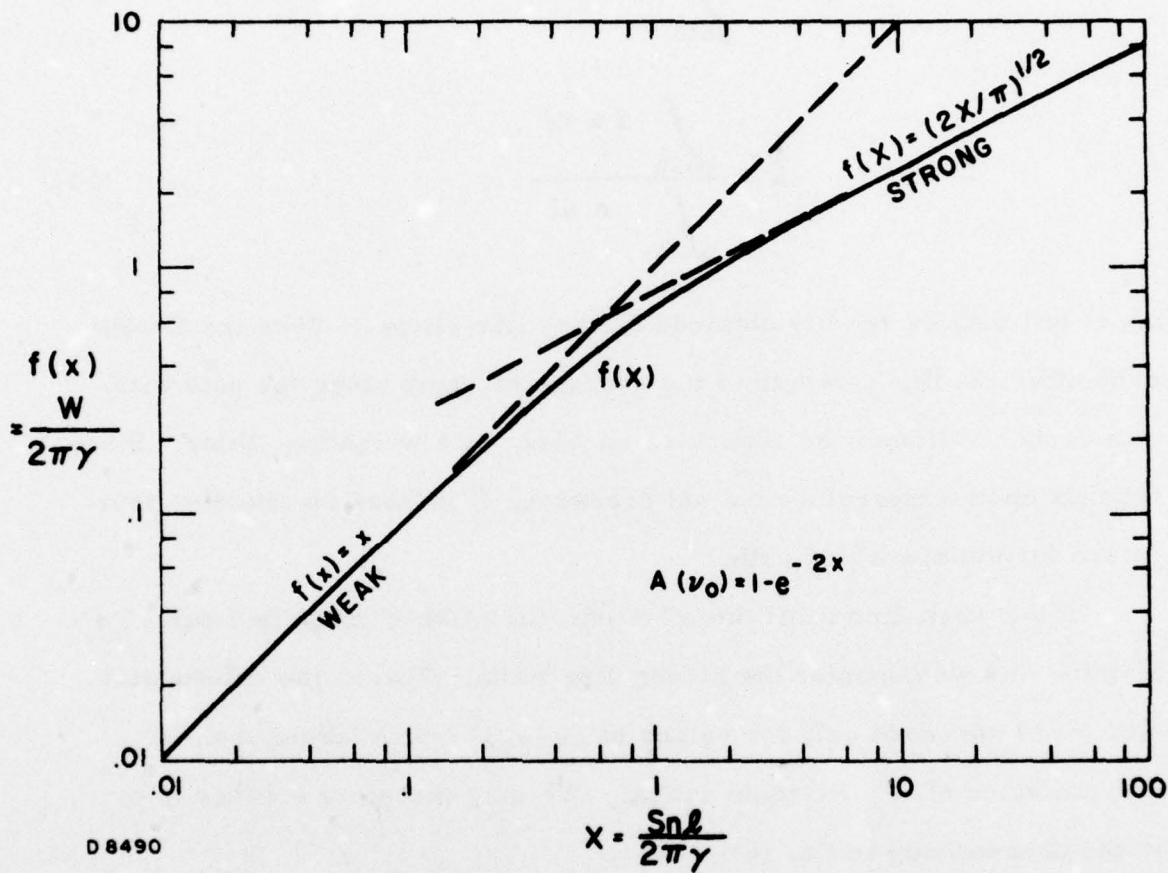
$$\tilde{x} = \frac{\tilde{S} u}{2 \pi \tilde{\gamma}}. \quad (10)$$

We seek  $\tilde{S}$  and  $\tilde{\gamma}$  such that the approximation becomes exact in the weak ( $\tilde{x} < .2$ ) and strong ( $\tilde{x} > 3$ ) line limits. For weak lines the exponent in Eq. (6) is very small relative to unity for all wavenumbers, and the exact equivalent width becomes

$$\begin{aligned} W &= \int_{\text{line}} \left\{ \int_{\text{path}} \frac{1}{\pi} \frac{S \gamma du}{(\nu - \nu_0)^2 + \gamma^2} \right\} d\nu \\ &= \int_{\text{path}} \left\{ \int_{\text{line}} \frac{1}{\pi} \frac{S \gamma d\nu}{(\nu - \nu_0)^2 + \gamma^2} \right\} du \quad (11) \\ &= \int_{\text{path}} S du \quad (\text{exact, weak}) \end{aligned}$$

For weak lines, we know that  $f(\tilde{x}) \cong \tilde{x}$ , so the Curtis-Godson approximation becomes, from Eqs. (9) and (10),

$$W = \tilde{S} u. \quad (\text{C.G., weak}) \quad (12)$$



D 8490

Figure 2. Curve of Growth for a Lorentz (Collision-Broadened) Spectral Line

For the approximation to be exact in the weak line limit, comparison of Eqs. (11) and (12) shows that the following relation is sufficient:

$$\tilde{S} u = \int_{\text{path}} S du, \quad (13)$$

or

$$\tilde{S} = \frac{\int_{\text{path}} S n dl}{\int_{\text{path}} n dl} \quad (14)$$

(This result may be readily obtained for any line shape.) Thus the Curtis-Godson effective line strength is the average strength along the path with  $n$ , the concentration of the absorbing species, as a weighting factor. Since  $S$  depends upon temperature but not pressure,  $\tilde{S}$  defines an effective temperature for the absorbing path.

In the weak-line limit the effective line width  $\tilde{\gamma}$  cancelled out. To determine this we consider the strong-line limit. There, the exponential in Eq. (6) is non-zero only for values of  $(\nu - \nu_0)^2$  much larger than the maximum value of  $\gamma^2$  (extreme wings). We may therefore replace  $\gamma$  by  $\tilde{\gamma}$  in the denominator in Eq. (6):

$$W = \int_{\text{line}} \left\{ 1 - \exp - \frac{1}{\pi} \frac{\int_{\text{path}} S \gamma du}{(\nu - \nu_0)^2 + \tilde{\gamma}^2} \right\} d\nu \quad (15)$$

(exact, strong)

Comparing Eqs. (8) and (15) we see that the Curtis-Godson approximation is exact in the strong-line limit if

$$\tilde{S} \tilde{\gamma} u = \int_{\text{path}} S \gamma du \quad (16)$$

or

$$\tilde{\gamma} = \frac{\int_{\text{path}} \gamma S n \, dl}{\int_{\text{path}} S n \, dl} \quad (17)$$

The Curtis-Godson effective line width  $\tilde{\gamma}$  is the weighted average line width, with  $S n$  as a weighting function. Because  $\gamma$  is proportional to pressure,  $\tilde{\gamma}$  might be considered as determining an effective pressure for the atmospheric column; the proportionality of  $\gamma$  to the inverse square root of temperature will have a minor effect in ordinary atmospheres.

Along a line of sight at an angle  $\theta$  from the horizon the incremental optical depth in any stratified atmosphere may be written  $du = n \, dl = n \, \csc \theta \, dh$ , where  $h$  is the height. Thus the total amount of absorber is

$$u = \csc \theta \int_{\text{path}} n \, dh = u_{\theta=90^\circ} \csc \theta = u_{\perp} \csc \theta \quad (18)$$

However, in the C-G parameters  $\tilde{S}$  and  $\tilde{\gamma}$  the  $\csc \theta$  factors which appear in both numerators and denominators of Eqs. (14) and (17) cancel, so that  $\tilde{S}$  and  $\tilde{\gamma}$  are independent of zenith angle.

Thus the C-G parameters may all be expressed in terms of integrals with respect to altitude. The weighting functions in the integrals for  $\tilde{S}$  and  $\tilde{\gamma}$  are not affected by the elevation angle of the optical path. In more general terms, the weighting is not affected by the opacity of the atmosphere. Opacity effects appear in the use of the C-G parameters to calculate atmospheric transmission, as in Eqs. (4), (9) and (10).

## 2.2 ACCURACY OF C. -G. APPROXIMATION IN AN EXPONENTIAL, MIXED, ISOTHERMAL MODEL ATMOSPHERE

The Curtis-Godson approximation is exact in the weak and strong line limits. For lines of intermediate strength, its accuracy may be checked for certain simple model atmospheres for which exact solutions may be readily obtained.

Let us consider a model atmosphere described as follows:

Total concentration:	$n_t = n_t(0) e^{-\ell/L_1}$	
Mole fraction of absorber:	$\chi = \text{const.}$	
Absorber concentration:	$n = \chi n_t = \chi n_t(0) e^{-\ell/L_1}$	(19)
Temperature:	$T = \text{const.}$	
Line strength:	$S = \text{const.}$	
Line half-width:	$\gamma = \gamma_0 n_t = \gamma_0 n_t(0) e^{-\ell/L_1}$	

Here the argument (0) refers to any reference altitude where  $\ell = 0$ .  $L_1$  is the e-folding distance along the upward-looking line of sight. It is related to the scale height  $H_1$  by  $L_1 = H_1 \csc \theta$  where  $\theta$  is the elevation angle. The line width  $\gamma_0$  refers to Standard Temperature and Pressure (STP). Species concentrations are to be measured in amagats, i. e., relative to the concentration at STP. In this discussion all gases are considered to have the same broadening power; the enhanced broadening power of  $H_2O$  is negligible at 3 km altitude or above.

### 2.2.1 Curtis-Godson Approximation

The effective Curtis-Godson parameters for a path through the present model atmosphere to outer space are readily calculated.

$$\begin{aligned}
 u &= \int_0^{\infty} n \, d\ell = \chi n_t(0) \int_0^{\infty} e^{-\ell/L_1} \, d\ell \\
 &= \chi n_t(0) L_1
 \end{aligned}
 \tag{20}$$

$$\tilde{S} = S$$

$$\tilde{\gamma} = \frac{\int_0^{\infty} \gamma n \, dl}{\int_0^{\infty} n \, dl} = \gamma_0 n_t(0) \frac{\int_0^{\infty} e^{-2l/L_1} \, dl}{\int_0^{\infty} e^{-l/L_1} \, dl} \quad (21)$$

$$= \gamma_0 n_t(0)/2 = \gamma(0)/2. \quad (22)$$

Thus in the Curtis-Godson approximation the equivalent line width is

$$W = 2\pi \tilde{\gamma} f(\tilde{x}) = 2\pi \frac{\gamma(0)}{2} f(2x_1), \quad (\text{C.G.})$$

where

$$\tilde{x} = \frac{\tilde{S} u}{2\pi \tilde{\gamma}} = 2 \frac{S \chi L_1}{2\pi \gamma_0} = 2x_1, \quad (23)$$

$$x_1 = \frac{S \chi L_1}{2\pi \gamma_0}. \quad (24)$$

Although the parameters  $u$ ,  $\tilde{S}$  and  $\tilde{\gamma}$  are sufficient for this analysis, it is instructive to introduce two additional parameters: the effective total density  $\tilde{n}_t$  and effective path length  $\tilde{l}$ , defined by the relations

$$\tilde{\gamma} = \gamma_0 \tilde{n}_t \quad (25)$$

and

$$u = \chi \tilde{n}_t \tilde{l}.$$

From Eqs. (20) and (22) we obtain

$$\tilde{n}_t = n_t(0)/2 \quad (26)$$

and

$$\tilde{l} = 2 L_1.$$

The effective total concentration (or pressure) is one-half the base-altitude value, while the effective path length is twice the scale length  $L_1$ . In the amount of absorber,  $u$ , these factors cancel (compare Eqs. (20) and (25)).

It should be observed that the total concentration  $n_t$  does not appear in Eq. (24), because it enters into both the numerator and denominator of the expression for  $\bar{x}$ .

For a finite path through this model atmosphere, the generalization of Eq. (22) leads to the result that the effective pressure for a finite path is the arithmetic average of the pressures at the two ends of the path.

### 2.2.2 Exact

For the exponential, mixed, isothermal model atmosphere Eq. (6) becomes

$$W = \int_{\text{line}} \left\{ 1 - \exp - \left[ \int_0^{\infty} \frac{1}{\pi} \frac{S_X \gamma_0 [n_t(0)]^2 e^{-2\ell/L_1} d\ell}{(\nu - \nu_0)^2 + \gamma_0^2 [n_t(0)]^2 e^{-2\ell/L_1}} \right] \right\} d\nu. \quad (27)$$

Making the substitutions

$$a = \frac{\nu - \nu_0}{\gamma_0}, \quad \beta = 2\ell/L_1,$$

and using Eq. (22), we simplify this to

$$\begin{aligned} W &= \gamma(0) \int_{-\infty}^{\infty} \left\{ 1 - \exp - \left[ x_1 \int_0^{\infty} \frac{e^{-\beta} d\beta}{a^2 + e^{-\beta}} \right] \right\} da \\ &= 2\gamma(0) \int_0^{\infty} \left\{ 1 - \exp - \left[ x_1 \ln \left( \frac{1+a^2}{a^2} \right) \right] \right\} da \\ &= 2\gamma(0) \int_0^{\infty} \left\{ 1 - \left( \frac{a^2}{1+a^2} \right)^{x_1} \right\} da \end{aligned}$$



This integral has been evaluated by Strong and Plass:<sup>1</sup>

$$W = 2 \pi^{1/2} \gamma(0) \frac{\Gamma(x_1 + 1/2)}{\Gamma(x_1)}. \quad (\text{Exact}) \quad (28)$$

The gamma function  $\Gamma(x)$  is defined for all positive values of  $x$ . For integral and half-integral values of the argument we have

$$\Gamma(n) = (n-1)!, \quad n = 1, 2, 3, \dots$$

$$\Gamma(n + 1/2) = \frac{1 \cdot 3 \cdot 5 \dots (2n-1)}{2^n} \Gamma(1/2)$$

$$\Gamma(1/2) = \pi^{1/2}$$

The asymptotes of the gamma function are such that Eqs. (23) and (28) agree for small and large  $x_1$ :

$$\begin{aligned} W &\rightarrow 2\pi \gamma(0) x_1, & x_1 &\rightarrow 0 \text{ (Weak)} \\ W &\rightarrow 2\gamma(0) (\pi x_1)^{1/2}, & x_1 &\rightarrow \infty \text{ (Strong)} \end{aligned} \quad (29)$$

The approximate and exact results for this model atmosphere are compared in Figure 3. The match is excellent. The percentage difference in effective line width  $W$ , given in Figure 4, peaks at 6% for  $x_1 = 0.5$  ( $\tilde{x} = 1$ ).

The 6% error will generally be an upper limit. Water vapor, which is of prime concern to us, has significant concentration over a smaller pressure range than the uniformly mixed absorber considered above, so the Curtis-Godson approximation will be more accurate than 6%. Also, the lines of concern to us are rather black ( $\tilde{x} \gtrsim 3$ ,  $x_1 \gtrsim 6$ ), so the expected error will be only ~ 1%. The error may be somewhat higher in the case of absorption by ozone, which is spread over a 20-km thick layer -- twice a scale height.

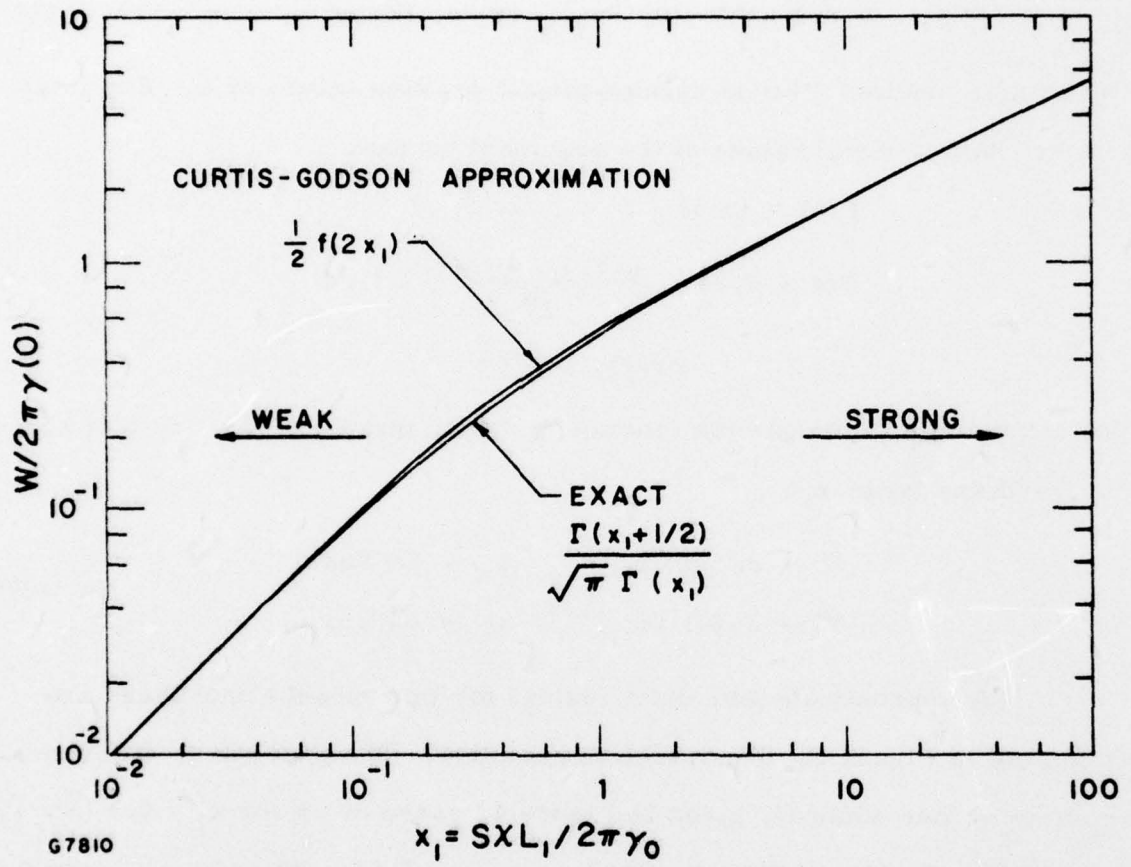


Figure 3. Equivalent Linewidth in Exponential Atmosphere

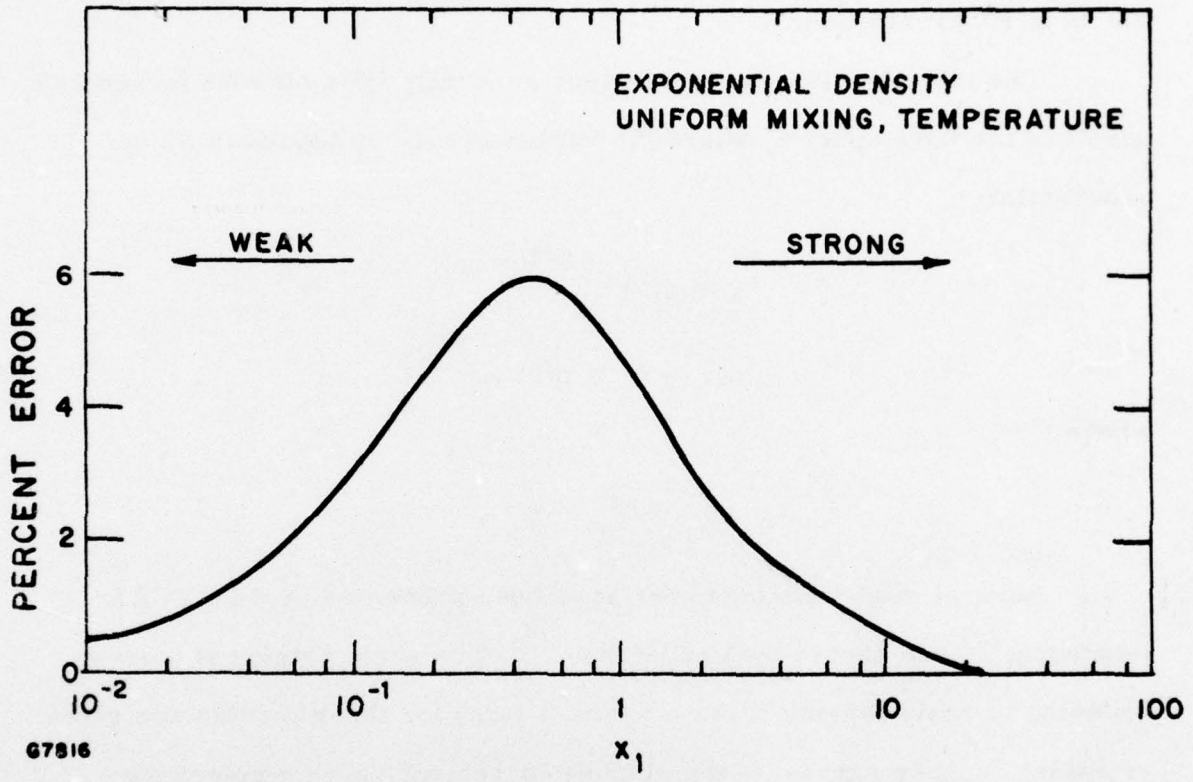


Figure 4. Error of Curtis-Godson Approximation

### 2.3 C.-G. APPROXIMATION APPLIED TO EXPONENTIALLY MIXED, ISOTHERMAL ATMOSPHERE

The model described above in Section 2.2 applies to absorption by species which are vertically mixed, such as CO<sub>2</sub> up to 50 km and N<sub>2</sub>O and CO up to 10 km altitude.

The mole fraction of water vapor generally falls off with increasing height in the troposphere, where the variation may be idealized by an exponential:

$$\begin{aligned}\chi &= \chi(0) e^{-\ell/L_2} \\ n &= \chi n_t = n(0) e^{-\ell/L_3}\end{aligned}\tag{30}$$

where

$$\frac{1}{L_3} = \frac{1}{L_1} + \frac{1}{L_2}.$$

Several model atmospheres have been presented in the AF'CRL Handbook, <sup>(2)</sup> and quoted by McClatchey. <sup>(3)</sup> The scale heights H (corresponding to scale lengths L for a vertical path) for these models are given in Table 1. They represent the altitude increment above a reference altitude h<sub>0</sub> in which the quantity shown falls by a factor of 1/e. In these models the mixing is not exactly exponential, as shown by the variation of scale height with altitude for the tropical model.

For isothermal model atmosphere in which the mole fraction of absorber varies exponentially the Curtis-Godson parameters are readily obtained:

TABLE 1. SCALE HEIGHTS IN MODEL ATMOSPHERES  
(AFCRL Handbook, 1965)

Model	Reference altitude $h_0$ (km)	1/e Height (km)		
		Total density	H <sub>2</sub> O mole fraction	H <sub>2</sub> O density
		H <sub>1</sub>	H <sub>2</sub>	H <sub>3</sub>
U. S. Standard	0.	9.3	3.6	2.6
Mid-latitude Winter	0.	8.8	4.1	2.8
Mid-latitude Summer	0.	9.6	2.9	2.2
Tropical	0.	9.8	3.2	2.4
	3.	9.2	1.9	1.6

$$\begin{aligned}
u &= n(0) L_3 = n(0) \frac{L_1 L_2}{L_1 + L_2} \\
\tilde{S} &= S(\text{const.}) \\
\tilde{\gamma} &= \gamma(0) \frac{L_1}{L_1 + L_3} = \gamma(0) \frac{L_1 + L_2}{L_1 + 2L_2}.
\end{aligned}
\tag{31}$$

Also, the use of Eq. (25) yields

$$\tilde{n}_t = \frac{L_1}{L_1 + L_3} n_t(0).$$

If we let  $L_2 \rightarrow \infty$ , the previous results for uniform mixing (Eqs. (20)-(22) and (26)) are obtained.

The exact solution for this model atmosphere could be obtained by numerical integrations, which we have not attempted. The error due to the use of the Curtis-Godson approximation should be less than that shown in Figure 4 which shows a maximum error of six percent.

## 2.4 C. -G APPROXIMATION APPLIED TO EXPONENTIALLY MIXED ATMOSPHERE WITH LINEAR TEMPERATURE VARIATION

Within the troposphere the temperature decreases with height. The variation along a line of sight with distance  $l$  may be approximated by a linear relation

$$T = T_0 + T' l \quad (32)$$

The strength of an atmospheric line, relative to the value at some reference temperature  $T_0$ , is

$$S(T) = S(T_0) \frac{Q_v(T_0)}{Q_v(T)} \left(\frac{T_0}{T}\right)^n \left[ \exp - \frac{hcE''}{k} \left(\frac{1}{T} - \frac{1}{T_0}\right) \right] \frac{1 - \exp - \frac{hcv}{kT}}{1 - \exp - \frac{hcv}{kT_0}} \quad (33)$$

For  $\text{CO}_2$ ,  $n = 1$ ; for  $\text{H}_2\text{O}$ ,  $n = 1.5$ . Also,  $E''$  is the lower level of the vibrational transition. At tropospheric temperatures the vibrational partition functions  $Q_v$  are close to unity, and the expression  $\exp - \frac{hcv}{kT}$  is very small (for  $\nu \gtrsim 500 \text{ cm}^{-1}$ ) compared with unity. Equation (33) may therefore be simplified to

$$S(T) = S(T_0) (T_0/T)^n \exp - \frac{hcE''}{k} \left(\frac{1}{T} - \frac{1}{T_0}\right) \quad (34)$$

We now evaluate the effect of this temperature variation on the Curtis-Godson effective line strength  $\tilde{S}$  in an atmosphere in which the density and absorber mole fraction decrease exponentially with altitude and the temperature decreases linearly. Substituting Eqs. (30) and (34) into Eq. (14) yields

$$\tilde{S} = \frac{S(T_0)}{L_3} \int_0^{l_\infty} \left(\frac{T_0}{T}\right)^n \left[ \exp - \frac{hcE''}{k} \left(\frac{1}{T} - \frac{1}{T_0}\right) \right] \left[ \exp - l/L_3 \right] dl \quad (35)$$

The upper limit is the distance at which  $T \rightarrow 0$ . We now introduce Eq. (32) and the parameters

$$A = hcE''/kT_0$$

$$B = -T_0/L_3 T'$$

$$a = T/T_0$$

to obtain

$$\tilde{S}/S_0 = B \exp(A-B) \int_0^1 a^{-n} \exp - \left(\frac{A}{a} - Ba\right) da \quad (36)$$

This expression has been evaluated numerically; the results are shown in Table 2.

The relevant values of the parameters may be obtained for the tropical atmospheric model. There we find that  $T' = -7 \sin \theta$  (deg K/km), where  $\theta$  is the elevation angle. Using  $T_0 = 296^\circ\text{K}$  (the reference temperature for the AFCRL compilation),  $L_3 = H_3 \csc \theta$ , and  $H_3 = 1.6$  km we have

$$A = E''/206 \text{ cm}^{-1}$$

$$B = 26$$

Inspection of values of  $E''$  for major  $\text{H}_2\text{O}$  lines in the 16-21  $\mu$  region reveals that most of them lie in the 550-1100  $\text{cm}^{-1}$  range, so that  $A = 2.7$  to 5.3 covers most cases. For  $\text{H}_2\text{O}$  lines Table 2 shows that  $\tilde{S}/S_0 = 0.85$  to 0.95.

This result indicates that the temperature dependence of the line strengths will not have a large effect on the Curtis-Godson parameter  $\tilde{S}$ .



TABLE 2. CURTIS- GODSON EFFECTIVE LINE STRENGTH S IN A NONISOTHERMAL ATMOSPHERE

$$\tilde{S}/S_0 = B e^{(A-B)} \int_0^1 \frac{1}{a^n} e^{-\left(\frac{A}{a} - B a\right)} da$$

	A	B = 25	35	50	70
n = 1	0.1	1.040	1.030	1.020	1.016
	2.5	.938	.959	.970	.982
	5	.853	.896	.924	.948
	7.5	.784	.841	.882	.917
n = 1.5	0.1	1.063	1.046	1.030	1.024
	2.5	.957	.973	.980	.989
	5	.869	.908	.933	.954
	7.5	.796	.851	.890	.923

## 2.5 EFFECTIVE PARAMETERS FOR THE WATER VAPOR CONTINUUM

The Curtis-Godson formalism is insufficient to describe the effect of the water vapor continuum. Additional parameters, derived in the present section, are required.

The atmospheric transmission by the water vapor continuum at any wavelength may be written

$$t = \exp - \int_{\text{path}} kn \, dl. \quad (37)$$

The absorption coefficient depends on both the water vapor and total concentrations:

$$k = k_0 (n + a n_t). \quad (38)$$

The coefficient  $a$  varies from only 0.001 in the 8 to 12  $\mu\text{m}$  window to about 0.02 at 20  $\mu\text{m}$ .<sup>(4)</sup>

In terms of the absorber mole fraction the transmission becomes

$$t = \exp - \int k_0 (\chi + a)\chi n_t^2 \, dl. \quad (39)$$

It is convenient to factor  $t$  to reflect the two terms of  $k$ :

$$t = t_s t_t,$$

where the effect of water vapor is given by

$$t_s = \exp - \int k_0 n^2 \, dl. \quad (40)$$

and the effect of the total concentration is given by

$$t_t = \exp - \int k_0 a n n_t \, dl. \quad (41)$$

We wish to obtain effective parameters which describe an equivalent uniform gas sample having the same transmission as the atmospheric path. First we treat the "self" factor given by Eq. (40). If the temperature along the path were constant, we could take  $k_0$  out of the integral:

$$\begin{aligned}
 t_s &= \exp - k_o \int n^2 dl \\
 &= \exp - k_o \int n du.
 \end{aligned}
 \tag{42}$$

The transmission of an equivalent sample is

$$t_s = \exp - k_o \tilde{n} u, \tag{43}$$

where of course  $u = \int n dl$ . Equating these expressions for  $t_s$  yields

$$\tilde{n} u = \int n du$$

or

$$\tilde{n} = \frac{\int n^2 dl}{\int n dl}. \tag{44}$$

Thus the effective water vapor concentration  $\tilde{n}$  is the average value of  $n$  along the path, with  $n$  also appearing as a weighting factor.

Introduction of temperature variation along the path leads us to a third effective parameter,  $\tilde{k}_o$ :

$$t_s = \exp - \tilde{k}_o \tilde{n} u. \tag{45}$$

For Eqs. (40) and (45) to yield the same result we must have

$$\tilde{k}_o \tilde{n} u = \int k_o n du$$

or

$$\tilde{k}_o = \frac{\int k_o n^2 dl}{\int n^2 dl}. \tag{46}$$

For this parameter, which determines an effective temperature for the path, the weighting factor is  $n^2$ .

We see that for calculation of  $t_s$ , any atmospheric path may be characterized by only three effective parameters:  $u$ ,  $\tilde{n}$  and  $\tilde{k}_o$ . The assumption of constant atmospheric temperature was merely a temporary

expedient to guide our definition of  $\tilde{n}$ . In contrast to the Curtis-Godson approach to a band of collision-broadened lines, no approximation is involved here.

An effective path length  $\tilde{l}$  could be used as an alternate to  $\tilde{n}$ . It is naturally defined as

$$\begin{aligned}\tilde{l} &= u/\tilde{n} \\ &= \frac{\left[ \int n \, dl \right]^2}{\int n^2 \, dl}\end{aligned}\tag{47}$$

In terms of this parameter, Eq. (45) becomes

$$t_s = \exp - \tilde{k}_o u^2/\tilde{l}.\tag{48}$$

To obtain effective parameters for  $t_t$ , an isothermal atmosphere is again temporarily invoked. Equation (41) becomes

$$\begin{aligned}t_t &= \exp - k_o a \int n_t \, du \\ &= \exp - k_o a \tilde{n}_t u\end{aligned}\tag{49}$$

The effective total concentration is evidently given by

$$\tilde{n}_t u = \int n_t \, du$$

or

$$\tilde{n}_t = \frac{\int n_t n \, dl}{\int n \, dl}.\tag{50}$$

The weighting factor is the same as for  $\tilde{n}$ .

A gas sample equivalent to a nonisothermal atmosphere has transmission

$$t_t = \exp - \tilde{k}_o a \tilde{n}_t u\tag{51}$$

Comparing Eq. (41) leads us to

$$(\widetilde{k_o a}) \tilde{n}_t u = \int k_o a n_t du$$

or

$$(\widetilde{k_o a}) = \frac{\int k_o a n_t n dl}{\int n_t n dl} \quad (52)$$

Here the weighting factor is the product  $n_t n$ .

These parameters may be evaluated for simple model atmospheres. If the temperature and mole fraction of water vapor are constant, and the total gas concentration falls off exponentially, as given by Eq. (19), then evaluation of Eqs. (44), (47) and (50) leads to the results

$$\begin{aligned} \tilde{n} &= n(0)/2 \\ \tilde{n}_t &= n_t(0)/2 \end{aligned} \quad (53)$$

and

$$\tilde{\ell} = 2L_1,$$

in agreement with Eq. (26).

If the mole fraction of water vapor falls off exponentially, as in Eq. (30), we obtain readily

$$\begin{aligned} \tilde{n} &= n(0)/2 \\ \tilde{n}_t &= n_t(0) \frac{L_1}{L_1 + L_3} \\ \tilde{\chi} &= \tilde{n}/\tilde{n}_t = \chi(0) \frac{L_1 + L_3}{2L_1} \\ \tilde{\ell} &= 2L_3. \end{aligned} \quad (54)$$

These results agree with Eq. (31) and the subsequent equation.

### 3.0 ATMOSPHERIC EMISSION-THEORY

In this section we derive relationships between absorption and emission intensities, with special emphasis on the apparent temperature of the atmosphere.

#### 3.1 LINE EMISSION

The atmospheric radiance (in watts/cm<sup>2</sup> - sr - cm<sup>-1</sup>) of an isolated spectral line may be written compactly as<sup>(5)</sup>

$$N_{\text{line}} = \int_{\text{path}} N_{\nu}^{\circ} (u) dW = \int_{\text{path}} N_{\nu}^{\circ} (u) \frac{dW}{du} du. \quad (55)$$

Remember that  $W$  is the equivalent width of the line, defined by Eq. (1).

If the atmosphere were isothermal, then the blackbody function  $N_{\nu}^{\circ}$  would be constant along the path, and we would have simply

$$N_{\text{line}} = N_{\nu}^{\circ} W. \quad (\text{Isothermal}) \quad (56)$$

For a nonisothermal atmosphere we may write an analog of Eq. (56):

$$N_{\text{line}} = N_{\text{eff}}^{\circ} W, \quad (57)$$

where the effective spectral blackbody radiance of the atmosphere is defined by

$$N_{\text{eff}}^{\circ} = \int_{\text{path}} N_{\nu}^{\circ} \frac{dW}{du} du / W. \quad (\text{Line}) \quad (58)$$

Here  $N_{\text{eff}}^{\circ}$  can be seen to be the blackbody radiance averaged over distance along the path, with  $ndW/du$  as weighting function, since  $W = \int (dW/du) ndl$ .

It is of interest to evaluate Eq. (58) under limiting conditions, using the Curtis-Godson approximation. In the weak-line limit, substitution of Eq. (12) into Eq. (58) yields

$$N_{\text{eff}}^{\circ} = \frac{\int_{\text{path}} N_{\nu}^{\circ}(u) \tilde{S}(u) du}{\int_{\text{path}} \tilde{S}(u) du}. \quad (\text{Weak line}) \quad (59)$$

In the weak line limit,  $N_{\text{eff}}^{\circ}$  is the blackbody radiance averaged over distance  $l$  along the path with  $\tilde{S}$  as a weighting function. Note that  $\tilde{S}(u)$  is an average over the finite path of optical depth  $u$ , the variable of integration.

In the strong line limit, where  $\tilde{\kappa} \gg 1$ , the Ladenburg-Reiche function has the asymptote  $f(\tilde{\kappa}) \cong (2\tilde{\kappa}/\pi)^{1/2}$ . From Eqs. (9) and (10) we then have

$$W(u) = 2 [\tilde{S}(u) \tilde{\gamma}(u) u]^{1/2}. \quad (\text{Strong line}) \quad (60)$$

This expression might be differentiated analytically with respect to  $u$  (see Ref. 5 for such an approach), but the result is complicated because of the dependence of  $\tilde{S}$  and  $\tilde{\gamma}$  upon  $u$ . In our numerical work we have instead calculated  $W$  vs  $u$  using Eq. (60), differentiated the result with respect to  $u$ , and then used Eq. (58) directly.

The error associated with the use of the Curtis-Godson approximation in determining  $dW/du$  may be greater than in determining  $W$  itself. We have not evaluated this error. It may be that the criteria for "weak" or "strong" are more stringent for  $dW/du$  than for  $W$ .

In the strong line limit one may be concerned that the integration indicated in Eq. (58) includes small values of  $u$  ( $u \lesssim 2\pi \tilde{\gamma}/\tilde{S}$ ) for which

the lines are weak or only moderately strong. This consideration is not a problem if  $N_{\nu}^0(u)$  is essentially constant for moderate values of  $u$ .

Then a value  $u_1 \gg 2\pi\tilde{\gamma}/\tilde{S}$  may be defined so that Eq. (58) becomes

$$\begin{aligned} WN_{\text{eff}}^0 &= \int_0^{u_1} N_{\nu}^0 \frac{dW}{du} du + \int_{u_1}^{u_{\text{end}}} N_{\nu}^0 \frac{dW}{du} du \\ &= N_{\nu}^0(u_1) W(u_1) + \int_{u_1}^{u_{\text{end}}} N_{\nu}^0 \frac{dW}{du} du. \end{aligned} \quad (61)$$

where  $u_{\text{end}}$  refers to the end of the path. Here  $W(u_1)$  is accurately given by the strong line limit, even though the details of the function  $dW/du$  in the range  $0 < u < u_1$  may be in error if Eq. (60) is used. In numerical cases of present interest we have determined that major  $H_2O$  lines become strong within a fraction of a kilometer, in which the temperature and hence  $N_{\nu}^0$  are indeed constant.

The effective temperature of the atmosphere ( $T_{\text{eff}}$ ) for line emission may be calculated from  $N_{\text{eff}}^0$  by inverting the Planck function. Equations (58) to (60) show that  $T_{\text{eff}}$  may be obtained from atmospheric temperature profiles and the Curtis-Godson parameters. The effective blackbody radiance and temperature of the atmosphere for line radiation are relatively insensitive to the elevation angle  $\theta$ . For example, suppose that the equivalent line width is proportional to some power of the optical depth  $u$ :  $W(u) = Au^n = Au_{\perp}^n \csc^n \theta$ . It is easy to show that the integral in Eq. (58) is also proportional to  $\csc^n \theta$ , so that  $N_{\text{eff}}^0$  is independent of  $\theta$ .

Actually we have  $n = 1$  for small values of  $u$  (weak-line limit) and  $n = 1/2$  for large values of  $u$  (strong-line limit). But in practical cases the lines are weak for such a small range of  $u$  that the integral in Eq. (61)



is accurately given by the assumption of  $n = 1/2$  for all values of  $u$ , as shown by Eq. (61) and the attendant discussion.

### 3.2 BAND EMISSION

Equation (4) tells us that atmospheric absorption is significant only if  $\bar{W}/\bar{d}$  (the ratio of equivalent line width to spacing), and hence the effective amount of overlapping of spectral lines in a band, is not small. Consequently, the foregoing analysis of emission from isolated lines needs to be generalized. The following is based in part on Ref. 5.

If we look at a band with spectral resolution that is fine compared to the widths of the lines, the spectral radiance of the gas along a path through the atmosphere is

$$N(\nu) = \int_{\text{path}} N_{\nu}^0 k(u) t(u) du, \quad (62)$$

where the  $k(u)$  is the total absorption coefficient due to all lines contributing at wavenumber  $\nu$ , and the spectral transmission through the optical depth  $u$  is

$$t(u) = \exp - \int_0^u k(u') du'.$$

Differentiation yields

$$\frac{dt(u)}{du} = - t(u) k(u)$$

so the high resolution atmospheric radiance may be written compactly

$$N(\nu) = - \int_{\text{path}} N_{\nu}^0 \frac{dt(u)}{du} du. \quad (\text{Band}) \quad (63)$$

Of more interest to us is the low resolution radiance  $N_\nu$  averaged over some spectral interval  $\Delta \nu$  containing many spectral lines:

$$N_\nu = \overline{N(\nu)} = - \int_{\Delta \nu} \left( \int_{\text{path}} N_\nu^0 \frac{dt}{du} du \right) d\nu / \Delta \nu.$$

Inverting the order of integration, and noting that  $N_\nu^0$  is constant within  $\Delta \nu$ , we rewrite this expression as

$$N_\nu = - \int_{\text{path}} N_\nu^0 \left( \int_{\Delta \nu} \frac{dt}{du} d\nu / \Delta \nu \right) du$$

or

$$N_\nu = - \int_{\text{path}} N_\nu^0(u) \frac{dt_\nu}{du} du, \quad (64)$$

where  $t_\nu$  is the spectral transmission averaged over  $\Delta \nu$ :

$$t_\nu = \int_{\Delta \nu} t d\nu / \Delta \nu.$$

The low resolution spectral radiance of the atmosphere may be written, analogously to Eq. (57), as

$$N_\nu = N_{\text{eff}}^0 \epsilon_\nu, \quad (65)$$

the product of the effective spectral blackbody radiance of the atmosphere and the spectral emissivity of the atmospheric path  $\epsilon_\nu = 1 - t_\nu$ .

Equations (64) and (65) then yield

$$N_{\text{eff}}^0 = - \frac{\int_{\text{path}} N_\nu^0 \frac{dt_\nu}{du} du}{1 - t_\nu}. \quad (\text{Band}) \quad (66)$$

This expression is convenient for numerical calculations.  $N_{\text{eff}}^0$  is the

blackbody spectral radiance averaged over distance, with  $n dt_{\nu}/du$  as weighting function. This may be shown more explicitly:

$$N_{\text{eff}}^{\circ} = \frac{\int_{\text{path}} N_{\nu}^{\circ}(u) \frac{dt_{\nu}}{du} du}{\int_{\text{path}} \frac{dt_{\nu}}{du} du} \quad (\text{Band}) \quad (67)$$

In a spectral band described by the statistical model, we have  $t_{\nu} = \exp - \bar{W}/\bar{d}$ . Substitution into Eq. (66) yields

$$N_{\text{eff}}^{\circ} = \frac{\int_{\text{path}} N_{\nu}^{\circ} \frac{d\bar{W}}{du} [\exp - \bar{W}/\bar{d}] du}{\bar{d} (1 - \exp - \bar{W}/\bar{d})} \quad (68)$$

If the effect of overlapping is negligible,  $\bar{W}/\bar{d} \ll 1$ , and this expression reduces to Eq. (58), which describes the nonoverlapping line case.

For a band of lines we have shown that the effective blackbody temperature of the atmosphere may be calculated from temperature profiles and the variation of atmospheric transmission along the line of sight.

In the case of emission from isolated lines, we saw that the effective temperature is independent of elevation angle if the equivalent line width  $W$  is proportional to some power of the optical depth ( $u^n$ ). The angle independence obtains even if  $n$  is dependent upon altitude, provided that variation of the local temperature is negligible in the range of altitudes in which  $n$  varies (which is the case under conditions of interest here). We have not succeeded in demonstrating any theorems concerning the angle independence of effective temperature for band radiation.

#### 4.0 ABSORPTION AND EMISSION PARAMETERS FOR A REAL TROPICAL ATMOSPHERE

Infrared transmission through the atmosphere is significantly affected by temporal fluctuations in atmospheric conditions, especially water vapor content. The shape of the curve of water vapor mixing ratio vs altitude often departs considerably from the average. Measurements of the real atmosphere must be considered.

#### 4.1 TROPICAL METEOROLOGY

First we review some features of tropical atmospheres, <sup>(6)</sup> with special reference to the Hawaiian Islands area. Solar heating of the Earth's surface near the equator (intertropical convergence zone, ITCZ) produces an upward flow of air which then travels poleward and later returns downward in the 15-30° latitude belts, which include the Hawaiian Islands. Flow back to the ITCZ closes the loop. The downward flow velocity is typically 60 m/day at the 700 mb level, falling smoothly to zero at the surface.

At the higher altitudes this flow brings down dry air from above. Also, solar heating of the ocean surface below produces local unstable air masses which carry moisture upward and generate cumulus clouds. Between these masses the flow is downward. The combined effect of these flows in the lower altitudes is a net upward transport of moisture together with a net downward transport of air.

At an altitude of 2 to 5 km, the upward flow of moisture and the downward flow of dry air meet, producing a sharp step in the profile of absolute humidity, as seen in Figures 5 and 6. These steps are almost always at the same altitude as temperature minima or inversions, shown in Figure 7. The humidity step is generally stable in the stratified atmosphere found in the summer (Figures 5 and 6), when the meteorology in the Hawaiian area is dominated by the ENE trade wind; hence this phenomenon is termed a trade-wind inversion. This inversion usually marks the tops of cumulus clouds. The step in the moisture profile is preserved because moisture which rises up into the inversion layer generally condenses, sometimes in the form of "inversion" stratus or stratocumulus clouds. (7) (Occasional penetration is marked by "chimney clouds".) Thus the upper dry layer stays dry. As we follow the trade wind from the Northeast Pacific to the Hawaiian Islands, upward transport of moisture causes the thickness of the moist layer to increase, although the air flow is slightly downward.

This trade-wind dominated pattern also occurs at times in the winter. At other times large cyclonic disturbances dominate, giving rise to much greater vertical mixing. Figure 8 thus shows humidity steps in some profiles and widespread mixing or patchiness in the troposphere in others during the first half of January.

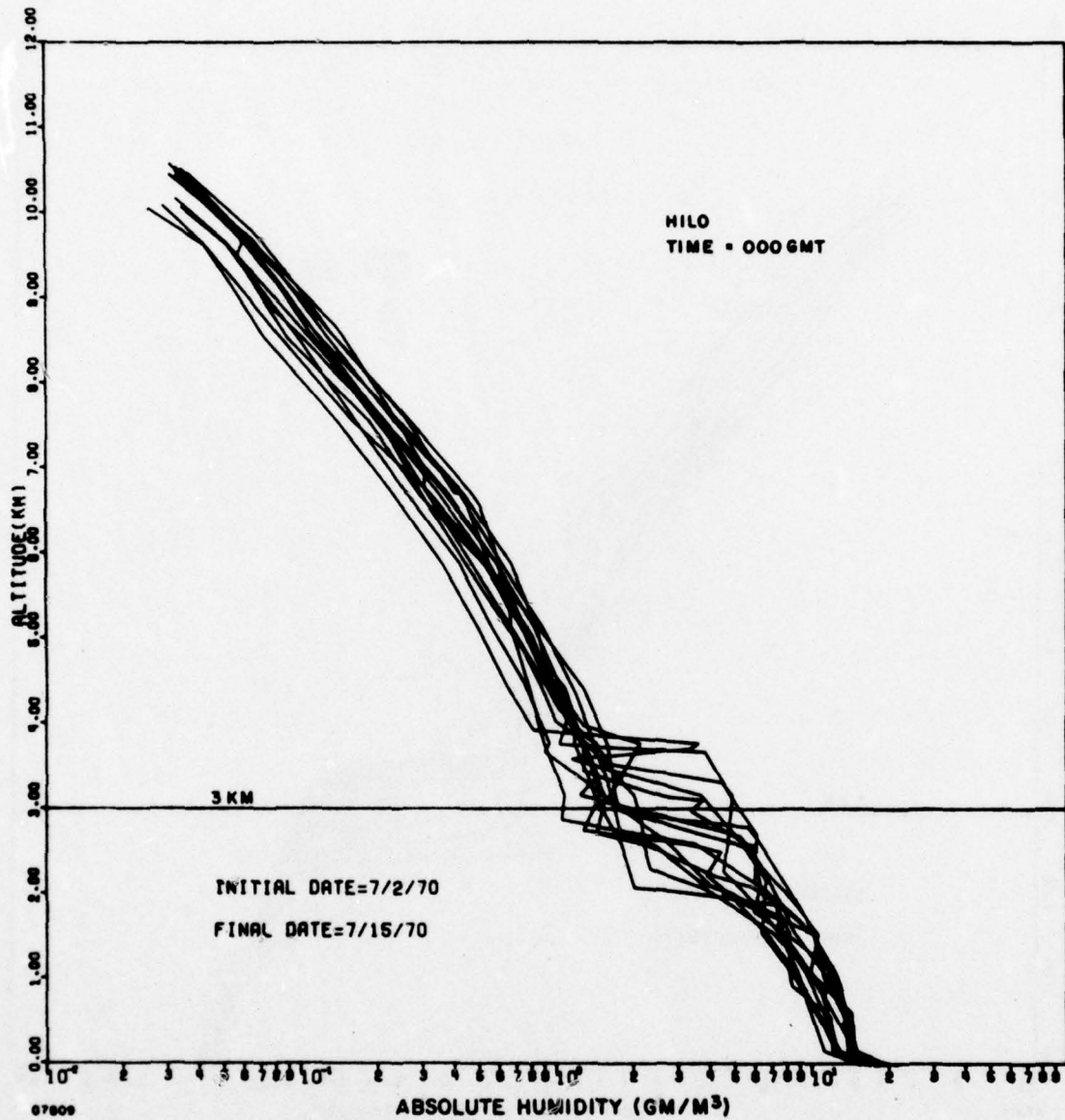


Figure 5. Humidity Profiles Derived from Rawinsonde Data for Hilo, Hawaii at Midnight GMT (July)

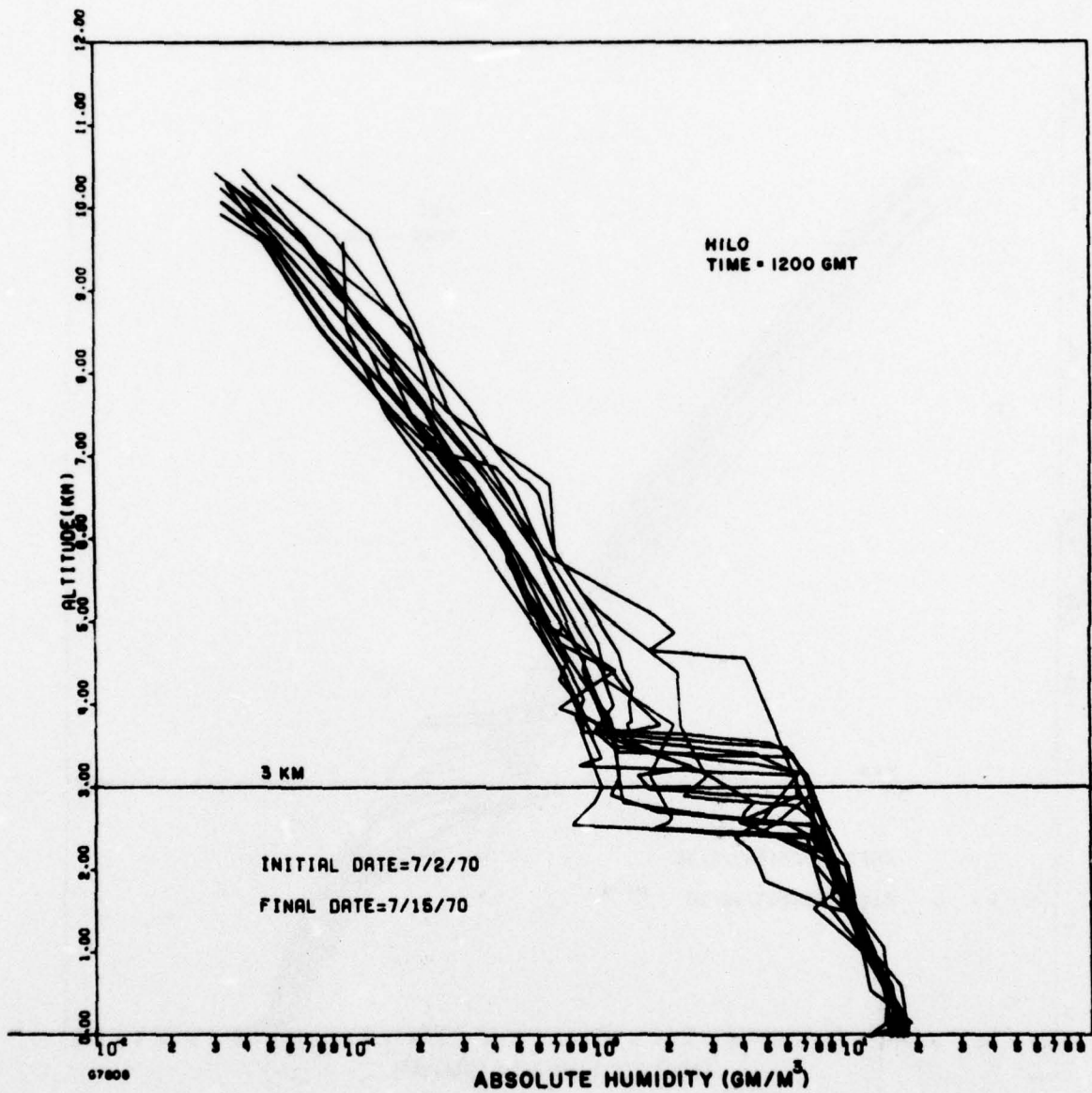


Figure 6. Humidity Profiles for Hilo at Noon GMT (July)

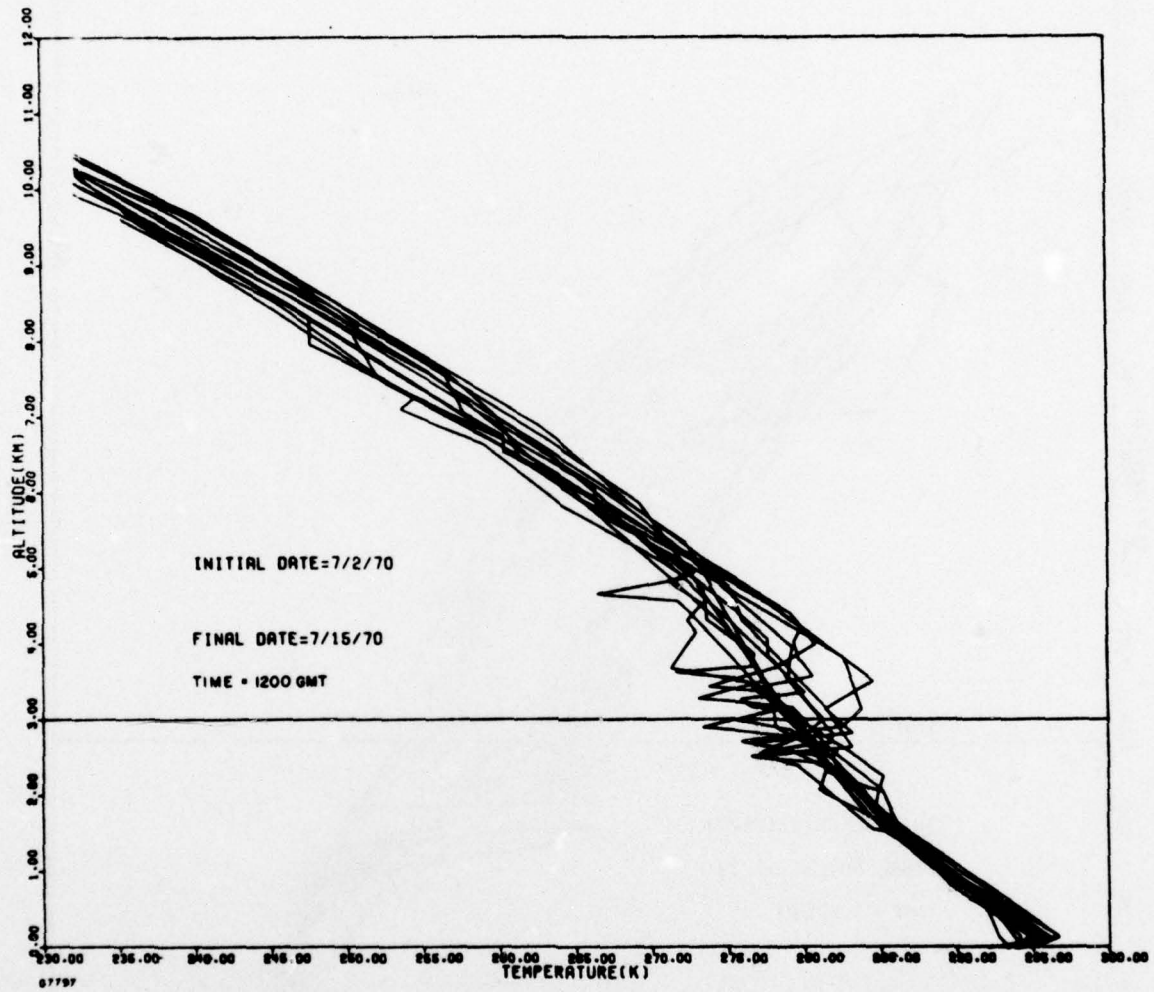


Figure 7. Temperature Profiles for Hilo at Noon GMT (July)



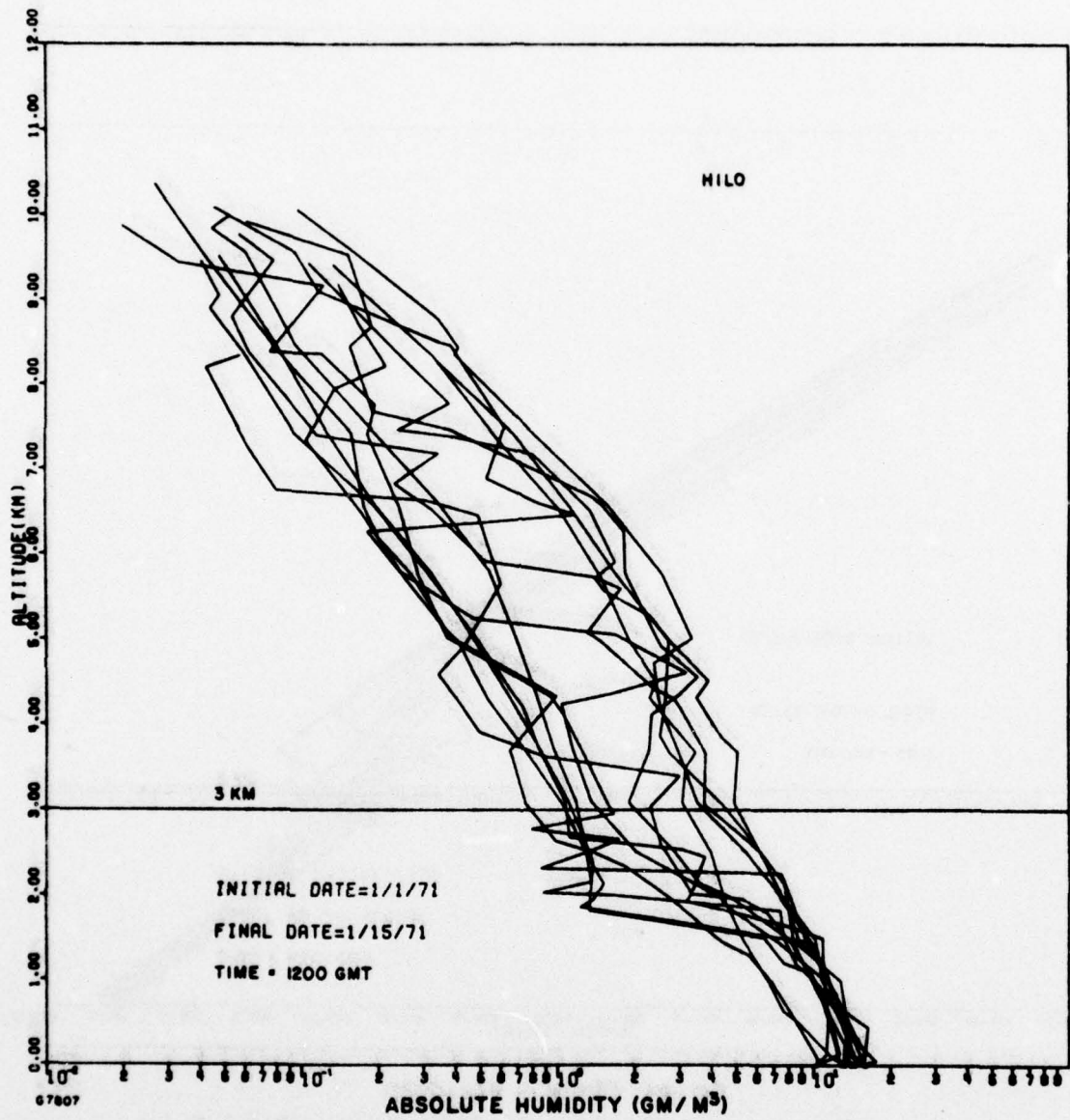


Figure 8. Humidity Profiles for Hilo at Noon GMT (January)

#### 4.2 ATMOSPHERIC RADIOSONDE DATA

Figures 5 to 8 illustrate radiosonde (balloon) measurements made twice daily at 0000 and 1200 hours GMT at more than 400 weather stations throughout the world and available on magnetic tapes from the NOAA National Climatic Center, Asheville, North Carolina. The tapes give relative humidity, temperature, and wind direction and speed at about 20 altitudes. We have analyzed data taken at Hilo on Hawaii Island, 160 km SE of AMOS Station on Maui.

Some caution should be observed in using the tapes. The National Weather Service hygristors<sup>(8)</sup> have reduced sensitivity at relative humidities less than 20%:

<u>Relative Humidity (%)</u>	
<u>Actual</u>	<u>NWS Hygristor Reading</u>
> 20	Actual $\pm$ 2%
20	20
15	18
10	16
5	14

Above the trade-wind inversion altitude, the atmosphere may be somewhat drier than indicated. During the last few years the NWS arbitrarily replaced all relative humidity readings below 20% by the default value of 19%. The data reported here is from earlier years, when this wrong-way "correction" was not used.

#### 4.3 CURTIS-GODSON PARAMETERS FOR ABSORPTION IN HAWAIIAN ISLANDS ATMOSPHERES

Looking at Figures 5, 6 and 8 we see that the integrated amount of water vapor,

$$u = \int_{3 \text{ km}}^{10 \text{ km}} n_{\text{H}_2\text{O}} dh,$$

above 3 km altitude varies over a wide range of values. In summer, the variation arises as the trade-wind inversion rises above or falls below the 3 km level. In winter, storms intermittently raise water vapor into the upper troposphere which is otherwise quite dry.

The history of the amount of water vapor,  $u$ , above 3 km at Hilo is shown in Figures 9 and 10 which show data for 2 p.m. and 2 a.m. local standard time, respectively. The extreme values differ by a factor of 50. The high values should be accurate within a few percent, but the low values may be somewhat high due to hygistor insensitivity.

The local water vapor density at 3 km altitude,  $\rho$ , correlates poorly with the total amount of water vapor above 3 km, as shown in Figures 11 and 12. If it is dry locally, it is dry above; but if it is humid locally there is wide scatter in the total water above, because the thickness of the humid layer above 3 km varies widely.

The other two Curtis-Godson parameters, the effective line strength  $\tilde{S}$  defined by Eq. (14) and the effective line width  $\tilde{\gamma}$  defined by Eq. (17), have been evaluated using Eq. (34) and the expression

$$\gamma = \gamma_0 (p/p_0) (T_0/T)^{1/2}. \quad (69)$$

Here  $p$  is the total atmospheric pressure. Self-broadening may be neglected above 3 km. Figures 13 and 14 show  $\tilde{S}/S_0$  and  $\tilde{\gamma}/\gamma_0$  for the Hilo radiosonde data above 3 km. The subscripts ( )<sub>0</sub> refers to STP.

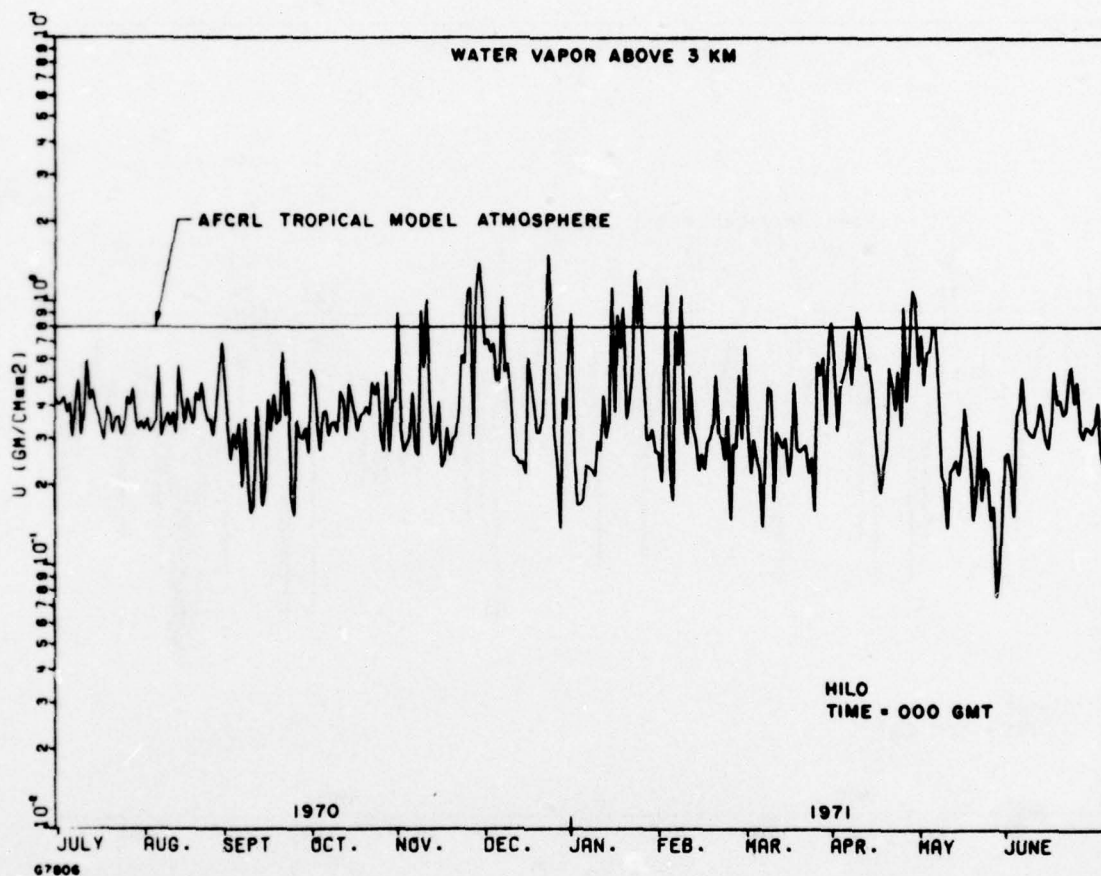


Figure 9. Amount of Water Vapor Above 3 km for Hilo at Midnight GMT (1970-71)

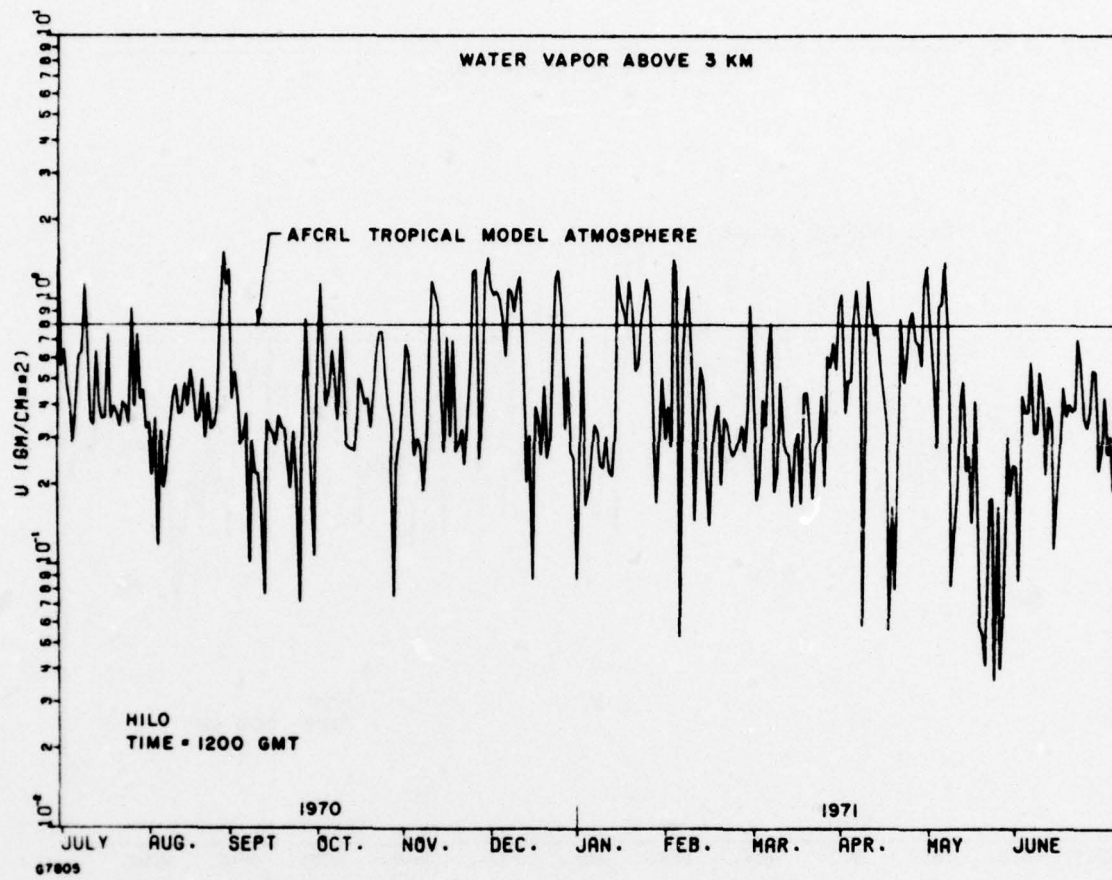


Figure 10. Amount of Water Vapor Above 3 km for Hilo at Noon GMT (1970-71)

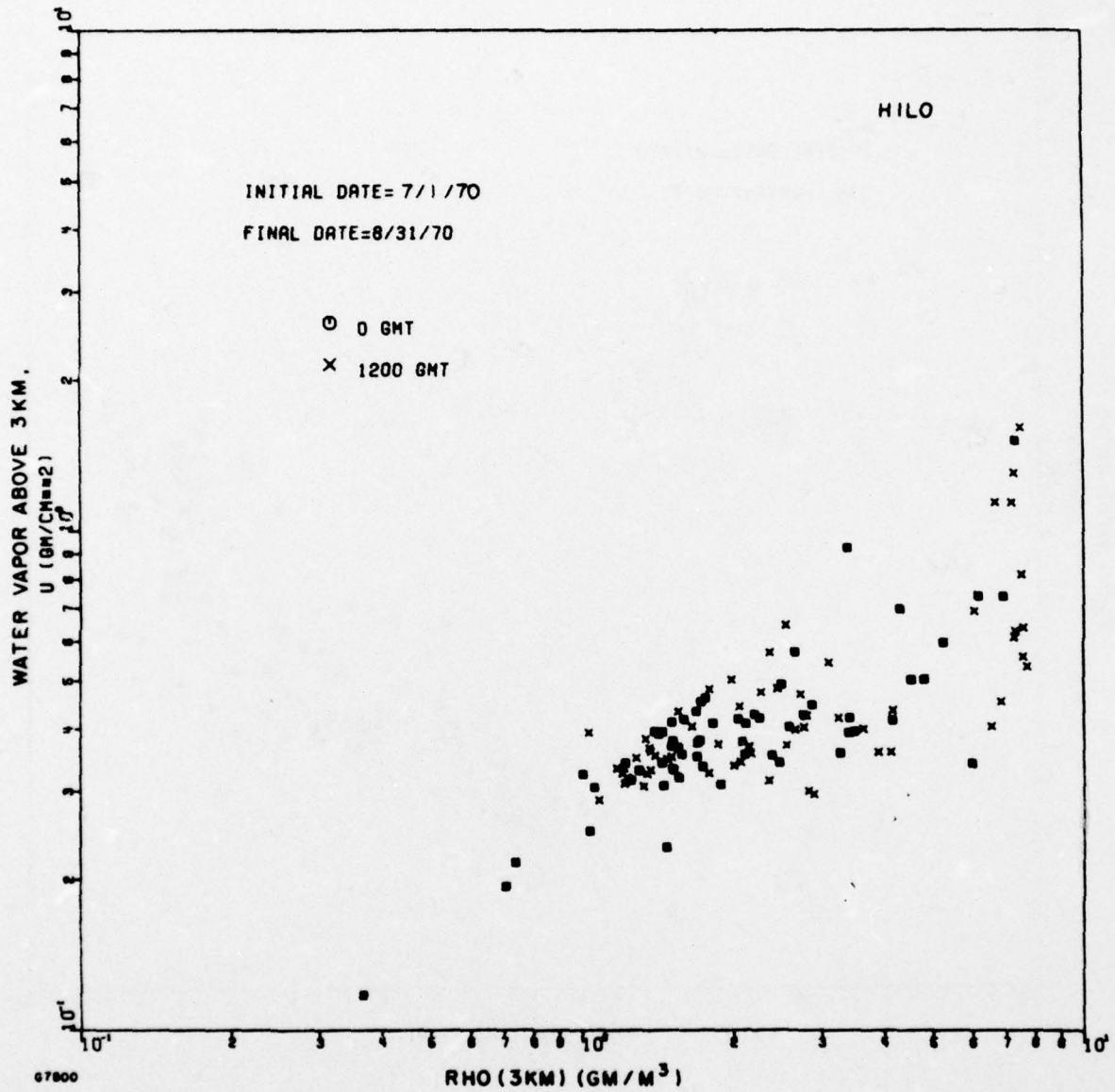


Figure 11. Total Amount of Water Vapor Above 3 km vs Absolute Humidity at 3 km for Hilo (Summer)

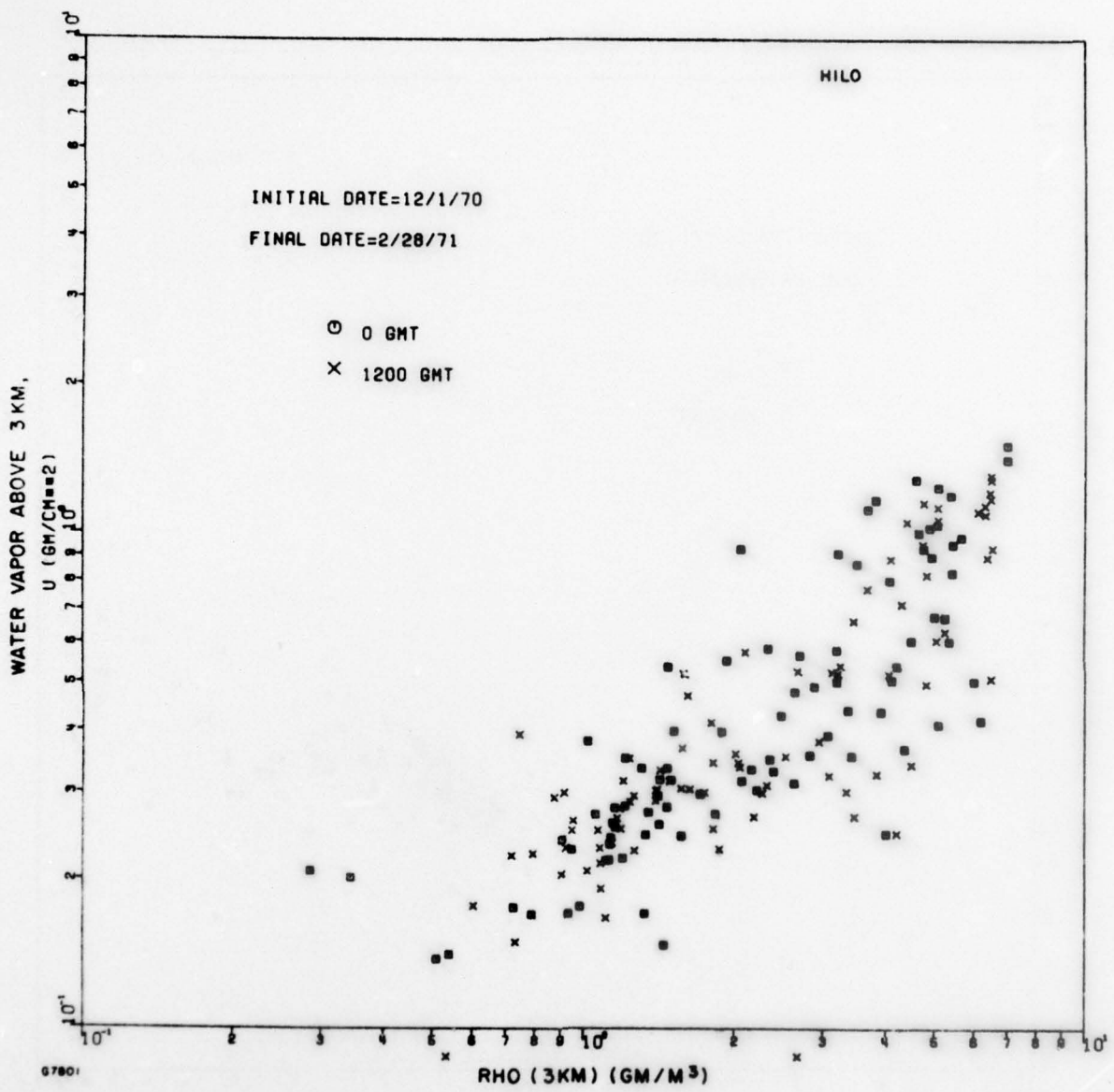


Figure 12. Total Amount of Water Vapor Above 3 km vs Absolute Humidity at 3 km for Hilo (Winter)

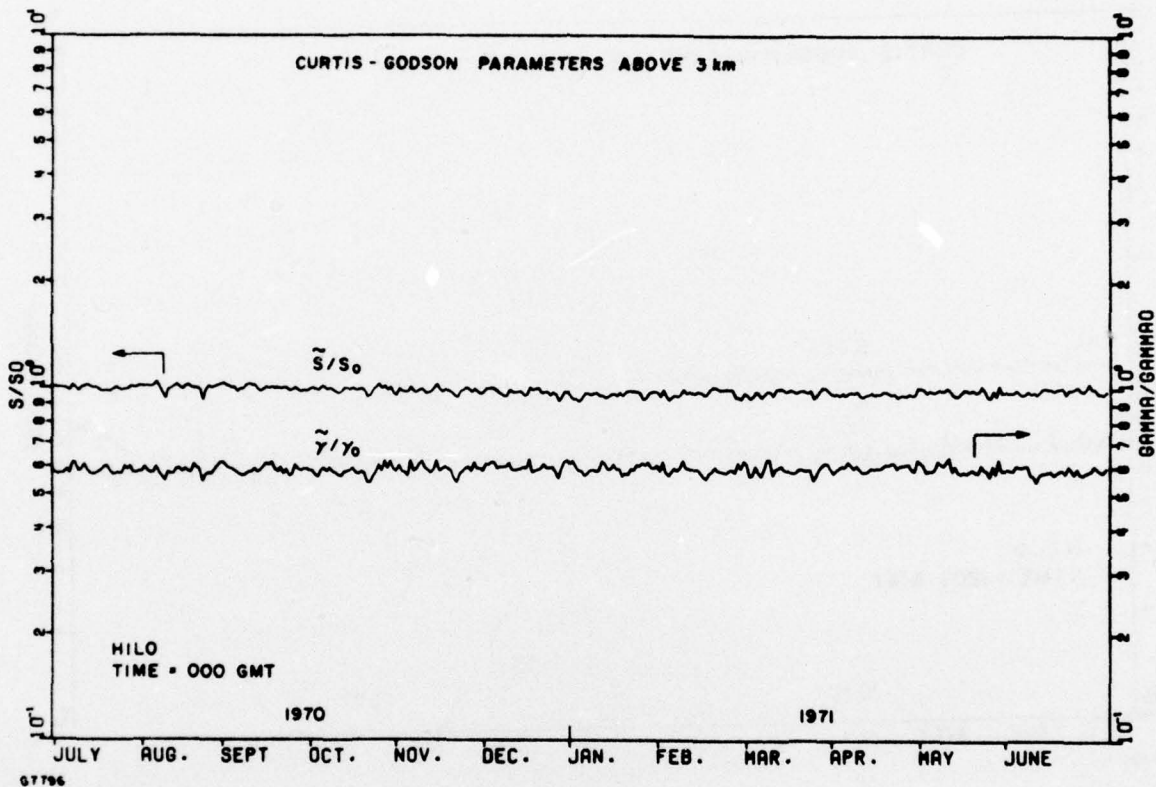
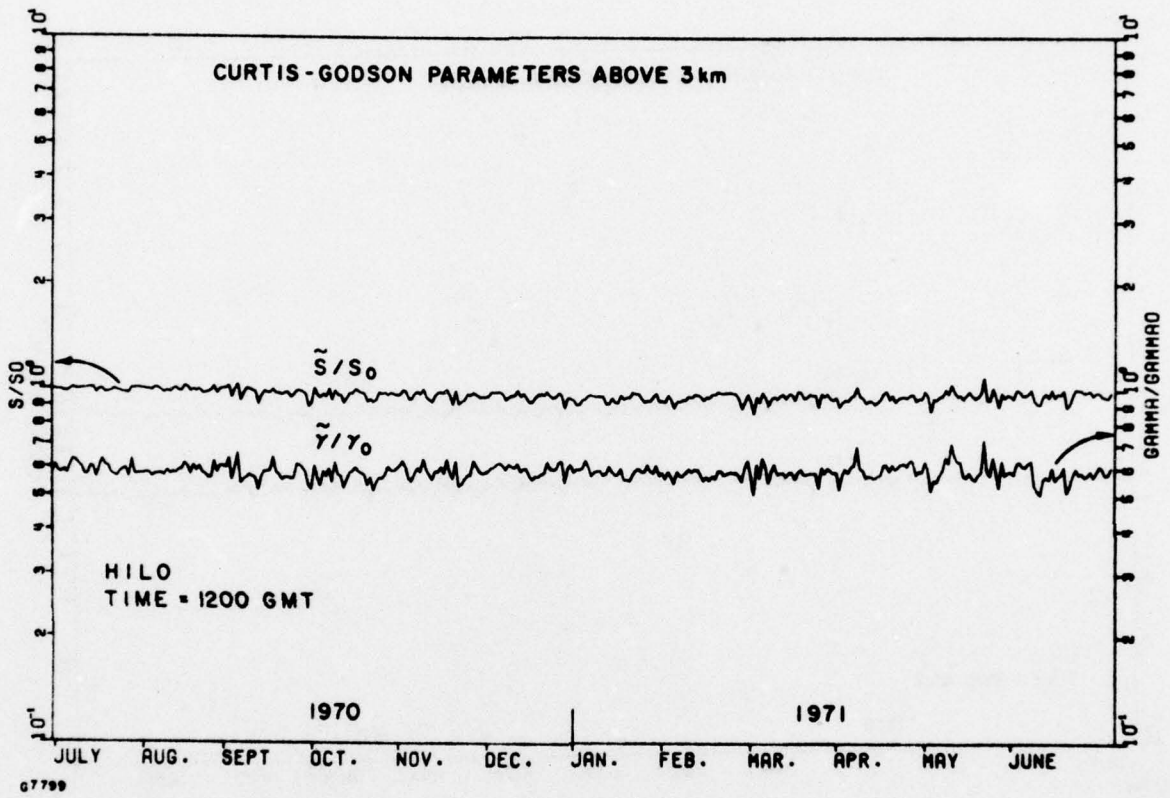


Figure 13. History of Effective Line Strength ( $S$ ) and Width ( $\gamma$ ) Above 3 km for Hilo at Midnight GMT (1970-71)





**Figure 14. History of Effective Line Strength (S) and Width (γ) Above 3 km for Hilo at Noon GMT (1970-71)**

These calculations are for a lower energy level  $E'' = 800 \text{ cm}^{-1}$ , which is typical of the strong  $\text{H}_2\text{O}$  lines found in the 16-21  $\mu\text{m}$  window. Varying  $E''$  from 550 to 1100  $\text{cm}^{-1}$  changes  $\tilde{S}/S_0$  and  $\tilde{\gamma}/\gamma_0$  only by 1-2%.

In contrast to the fluctuating  $u$ , the parameters  $\tilde{S}$  and  $\tilde{\gamma}$  are seen to have very small diurnal or seasonal variations for this tropical location because the amount of water vapor appears in both the numerator and denominator of Eqs. (14) and (17). This means that we may make atmospheric absorption calculations assuming constant values for the effective temperature and pressure of the atmosphere above 3 km at Hilo. (In other calculations for temperate atmospheres  $\tilde{S}$  showed a  $\pm 10\%$  seasonal change.)

We conclude that the temporal variations in the atmospheric column of interest may be described by changes in a single parameter,  $u$ , as far as absorption by bands of water vapor lines is concerned. For the water vapor continuum it is possible that additional parameters such as  $\tilde{n}$  or  $\tilde{n}_t$ , defined by Eqs. (44) and (50), might be necessary for complete description of local meteorological conditions.

#### 4.4 RELEVANCE OF HILO DATA TO MT. HALEAKALA

Located on the northeast shore of the Island of Hawaii, Hilo is generally on the windward side of Mauna Loa and Mauna Kea (elevations 4.2 km). (The wind at 1.5 km comes only rarely from more than  $\pm 45^\circ$  away from the east - Ref. 9, Figure 63.) Thus, the Hilo rawinsonde profiles represent the interisland trade wind atmosphere, relatively free from orographic influences.

Radiative heating and cooling of the surface of the mountains (if not hindered by cloud cover) generate local upslope winds by day and downslope winds by night. Mendonca<sup>(10)</sup> has studied these winds at Mauna Loa Observatory, located at 3.4 km altitude on the windward side of Mauna Loa. He found the nocturnal downslope wind, which lasts until about 0730 local time, had a thickness of only about 50 m. The thickness of the upslope wind grew to some 500 m by local noon - the result of unstable convective mixing and greater fetch. The atmosphere over the open ocean can be modified close to a mountain in the Hawaiian Islands, but the region affected will be very thin, especially at the top of a mountain at night.

These thermally generated local mountain winds are to be distinguished from the mechanical disturbance of the trade-wind flow due to the mountains. Because their slopes are very steep, the trade wind will generally flow around Mauna Loa and Mt. Haleakala more than over them (Ref. 6, pp. 105-6). The step in humidity profile has been found at the surface of Mauna Loa at an altitude close to that in the rawinsonde data.<sup>(11)</sup>

#### 4.5 EMISSION PARAMETERS FOR HAWAIIAN ISLANDS ATMOSPHERES

In Section 3.1 we showed that the radiance of the atmosphere from an isolated spectral line ( $N_{\text{line}}$ ) can be obtained as the product of the effective blackbody radiance ( $N_{\text{eff}}^{\circ}$ ) and the equivalent line width ( $W$ ). The last variable depends upon the absorption parameters  $u$ ,  $\tilde{S}$  and  $\tilde{\gamma}$ , whose variations we already have displayed. Here, we consider the variability of  $N_{\text{eff}}^{\circ}$ .

This parameter has been calculated for water vapor emission using the measured atmospheric profiles 3 km and more above Hilo, Hawaii. Numerical studies, presented below, show that the significant emission comes from strong  $\text{H}_2\text{O}$  lines, so we use Eqs. (58) and (60); for comparison we also evaluate Eq. (59) based upon the weak line assumption. These results have little dependence on the parameters of the spectroscopic lines. The calculation involves determining only  $u$ ,  $\tilde{S}$  and  $\tilde{\gamma}$ , and then  $W$ , as functions of altitude, and we have already seen that  $\tilde{S}$  and  $\tilde{\gamma}$  are affected very weakly by the choice of  $E''$ , the lower energy level of the spectral line.

Figure 15 shows the history of  $N_{\text{eff}}^{\circ}$ , the effective spectral blackbody radiance of the atmosphere, at 1200 hours GMT. Inverting the Planck function yields the effective atmospheric temperature histories presented in Figure 16. In each figure the strong line assumption gives the upper curve, while the weak line assumption gives the lower. For the latter we "see" up to higher altitudes where the atmosphere is colder. The scales of these figures are quite expanded; a small deviation from strong line conditions would not introduce a significant error.

Referring to the upper curve of Figure 15, we see that  $N_{\text{eff}}^{\circ}$  has a seasonal (summer to winter) change of 10%, and short-term fluctuations

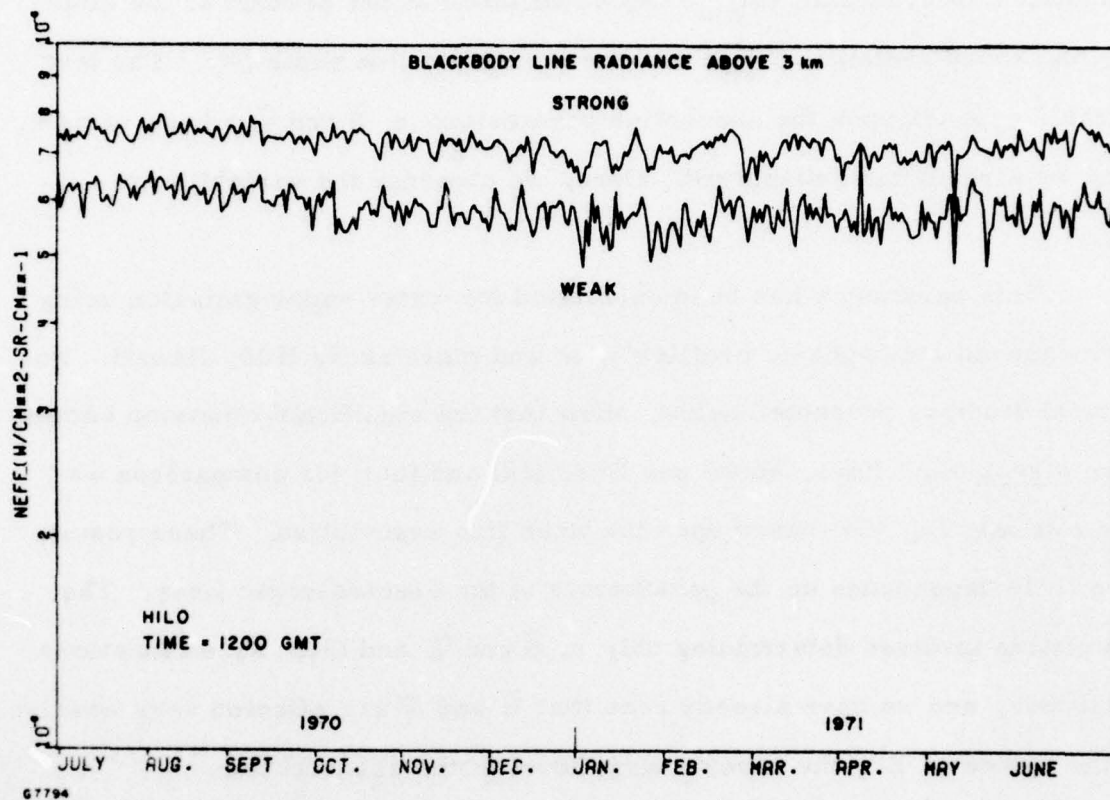


Figure 15. Effective Blackbody Spectral Radiance for Atmospheric Line Emission at 3 km Above Hilo

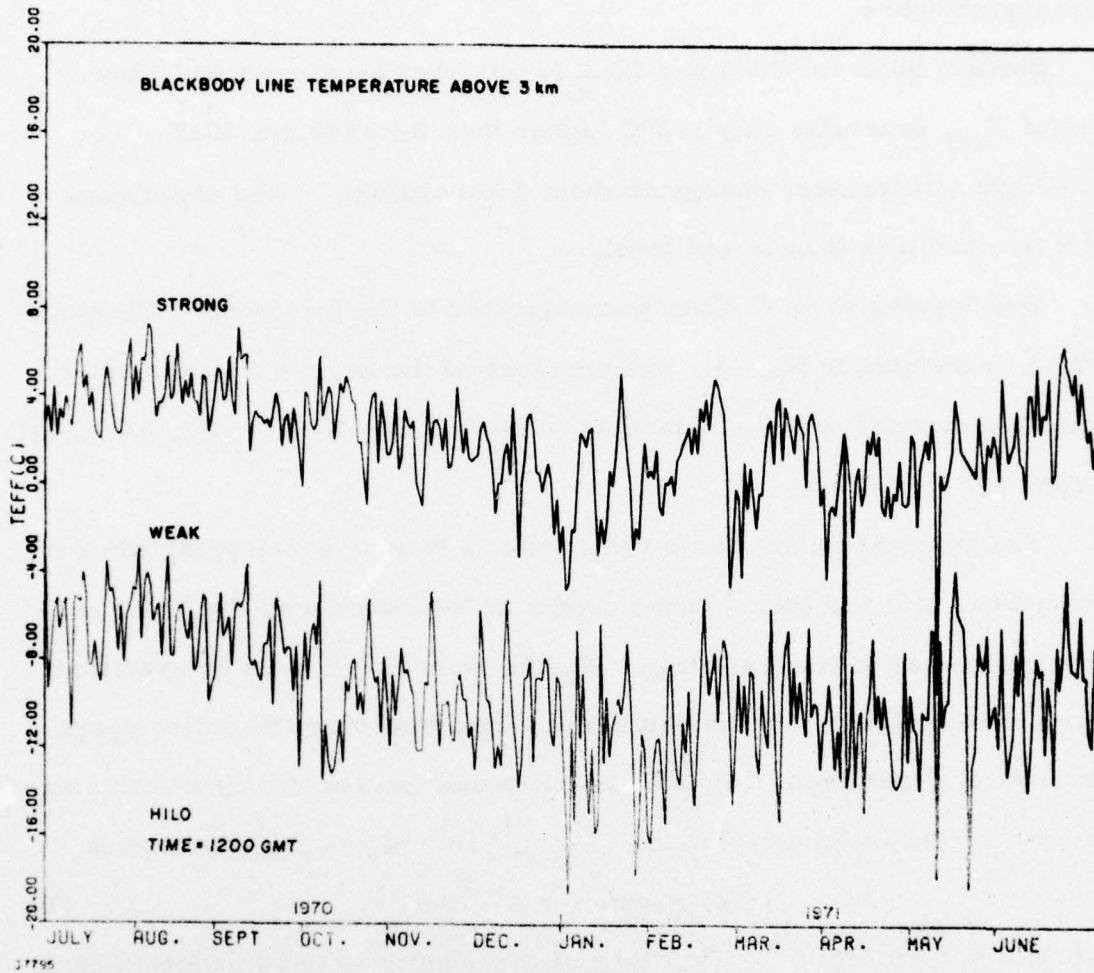


Figure 16. Effective Blackbody Temperature for Atmospheric Line Radiation, as seen from 3 km Above Hilo

of  $\pm 5\%$ . This is much smaller than the expected fluctuation of  $W$  (proportional to the square root of the highly variable  $u$ ) or  $N_{\text{line}}$ . This point will be elaborated below.

Similar plots for 0000 hrs GMT (2 pm local standard time) show values of  $T_{\text{eff}}$  generally only 1-2°C higher than for 1200 hrs GMT. The day-to-night temperature change at about 4 km altitude — the significant level — is much less than at sea level.

Overlapping of  $\text{H}_2\text{O}$  lines was neglected in the foregoing. The quantity  $\bar{W}/\bar{d}$ , presented in Eq. (4), is a measure of the degree of overlapping. In typical numerical cases of interest, we have found  $\bar{W}/\bar{d} \sim 1/2$ , so we will now consider this effect.

The spectral atmospheric radiance of a band of overlapping lines is given by Eqs. (65) and (66). These cannot be evaluated with the broad generality we applied to line radiation. The function  $t_v(u)$  must be specified. Numerical calculations, described below, show that over the entire range of amounts of water vapor ( $u$ ) to be encountered for reasonable zenith angles the transmission averaged over the 17-21  $\mu$  band may be represented as

$$t_v(u) = \exp - a u^{1/2}, \quad (70)$$

where  $a = 0.8 \text{ cm/gm}^{1/2}$ . This type of dependence is to be expected considering that the absorption is dominated by strong lines.

Using Eqs. (66) and (70) we obtain the history of the effect blackbody radiance of the  $\text{H}_2\text{O}$  band shown in Figure 17, and the effective atmospheric temperature in Figure 18. The results are difficult to distinguish from the strong-line curves of Figures 15 and 16. The effect of overlapping has a minimal effect on  $N_{\text{eff}}^0$  and  $T_{\text{eff}}$ .

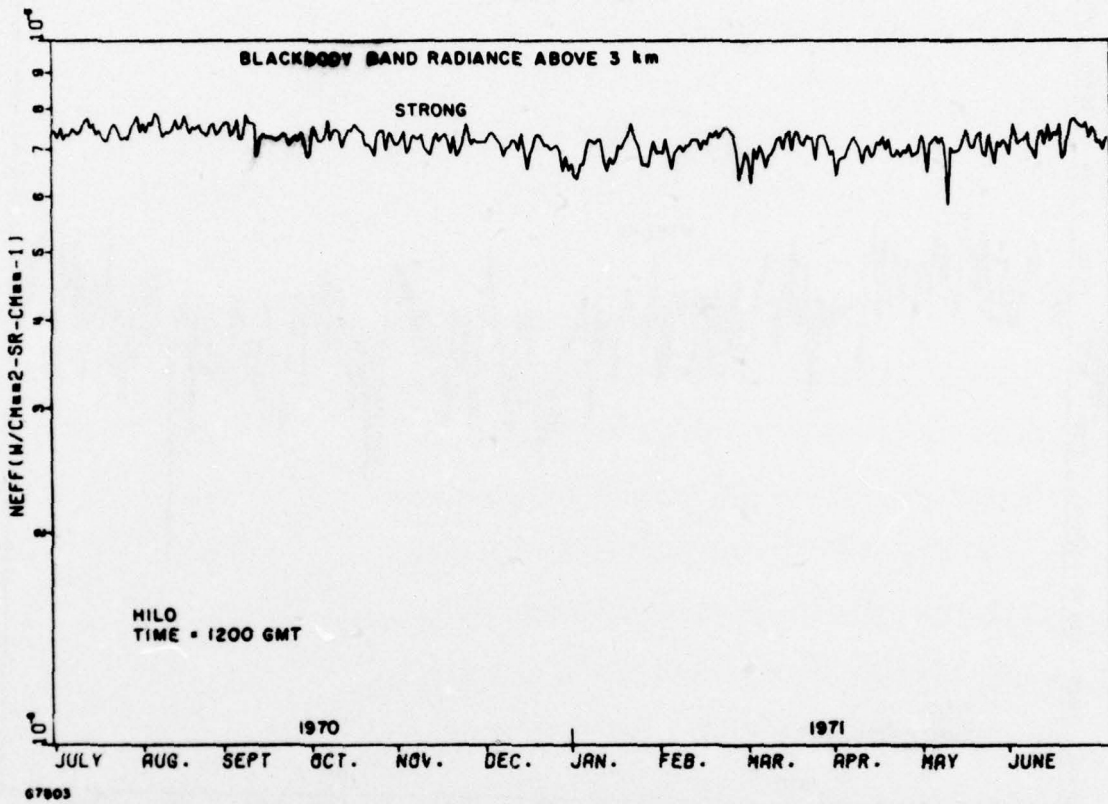


Figure 17. Effective Blackbody Spectral Radiance for Atmospheric Band Radiation at 3 km Above Hilo



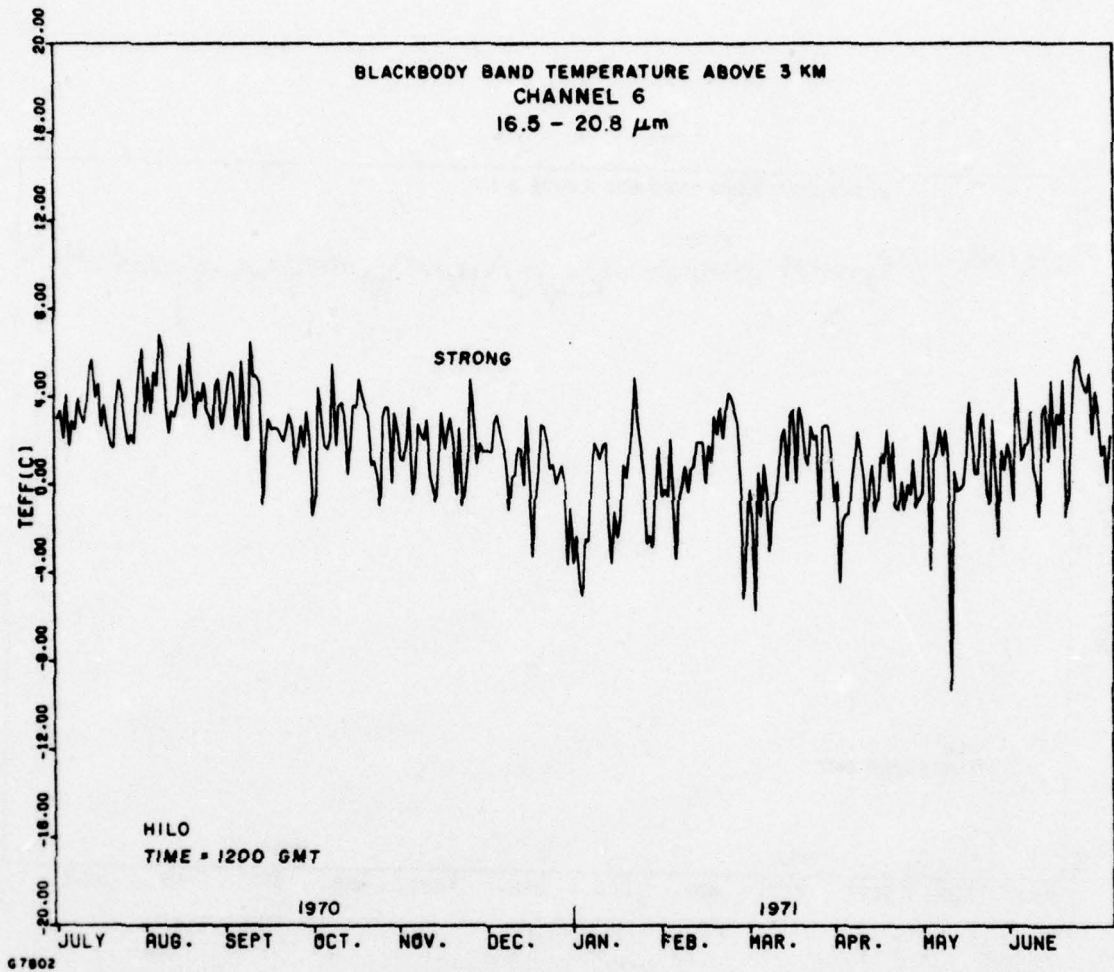


Figure 18 Effective Blackbody Temperature for Atmospheric Band Radiation, as seen from 3 km Above Hilo

The zenith angle of the optical path does not affect the effective black-body radiance for isolated lines; if  $W$  is proportional to some power of  $u$ , the numerator and denominator of Eq. (58) change with angle by equal factors. Since we have seen that overlapping of lines affects  $N_{\text{eff}}^{\circ}$  very little, it should be independent of zenith angle also for a band of lines. We have not performed detailed numerical tests of this conclusion.

The spectral radiance of atmospheric  $\text{H}_2\text{O}$  lines, averaged over the 16-21  $\mu\text{m}$  region, has been calculated using Eq. (63). The result, presented in Figure 19, shows considerable day-to-day fluctuations - much larger than those of  $N_{\text{eff}}^{\circ}$  in Figure 17. This means that the atmospheric  $\text{H}_2\text{O}$  band radiance is influenced much more by variations in the amount of water vapor overhead than by variations in the effective temperature of the water vapor.

Consequently, if we can perform real-time measurements of the atmospheric emission by  $\text{H}_2\text{O}$  lines, the data could be used to determine  $\epsilon_v$ , by assuming a constant  $N_{\text{eff}}^{\circ}$ , and thus the water vapor line transmission  $t_v = 1 - \epsilon_v$ .

This scheme can succeed even if in addition to  $\text{H}_2\text{O}$  line emission we have radiation from the  $\text{H}_2\text{O}$  continuum or from other sources, because Eqs. (62) - (66) can be rewritten in terms of the distance  $l$  instead of the optical depth  $u$ . However, cirrus clouds or aerosols which do not obey the relation  $t_v = 1 - \epsilon_v$  because of reflection or scattering could reduce the accuracy of this approach.

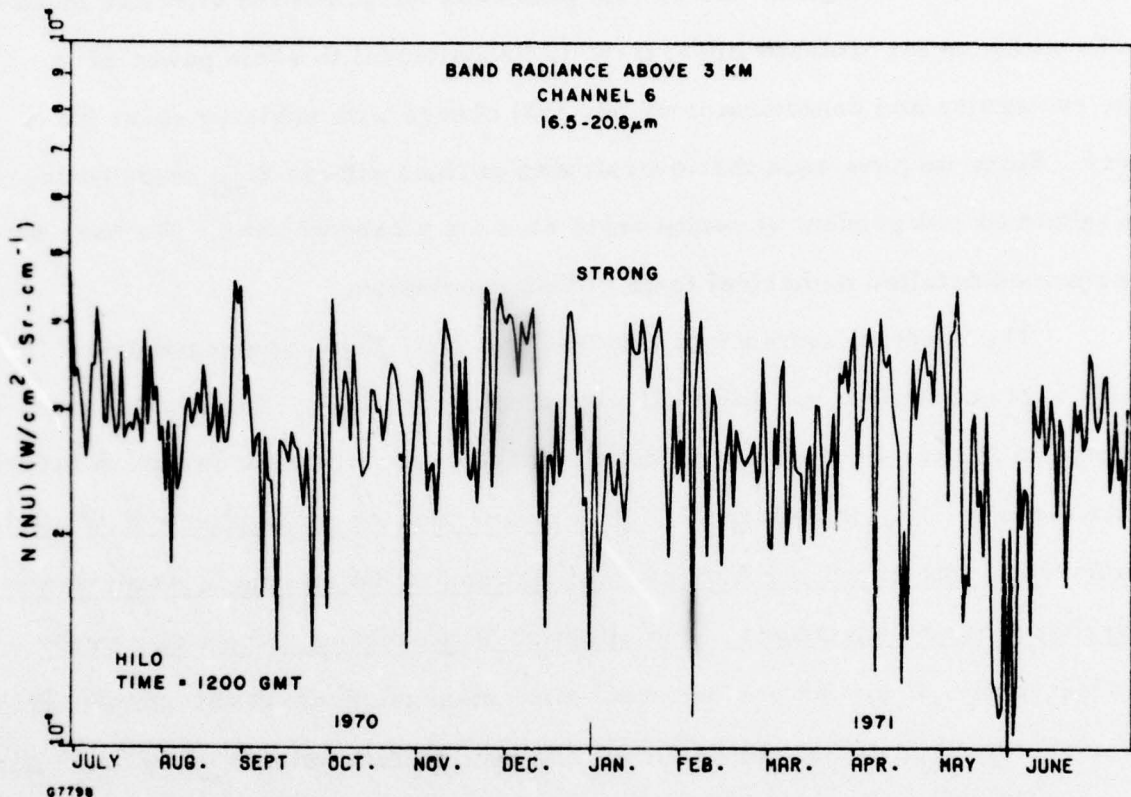


Figure 19. Spectral Band Radiance of Atmospheric Water Vapor Above 3 km at Hilo

## 5.0 ABSORPTION PREDICTIONS

In this section we present calculations of the atmospheric transmission along lines of sight extending from an altitude of 3 km to outer space, with elevation angle and amount of water vapor overhead as variable parameters.

### 5.1 SPECTROSCOPIC PARAMETERS

In addition to the Curtis-Godson parameters  $u$ ,  $\tilde{S}/S_0$  and  $\tilde{\gamma}/\gamma_0$ , obtained in Section 4 from radiosonde measurements of the Hawaiian Islands atmosphere, we use the AFCRL compendium of spectroscopic line parameters.<sup>(12)</sup> From this magnetic tape we read the line strength ( $S_0$ ), width ( $\gamma_0$ ) and wavenumber for each spectral line of the species of interest. Transmission by bands of lines was calculated using Eqs. (4), (9) and (10) and Figure 2.

For the H<sub>2</sub>O continuum, we use the data of Roberts, Selby and Biberman<sup>(4)</sup> and Burch, Gryvnak and Gates.<sup>(13)</sup> The latter indicates the temperature dependence of the absorption coefficient  $k_0$ . Equations (45), (49) and (54) were used to evaluate the water vapor continuum transmission. This means that we assumed an exponentially mixed atmospheric model for the continuum; the 1/e fall-off distance for H<sub>2</sub>O mole fraction was estimated from Eq. (31) and actual Hilo data (Figures 11 and 12). We found  $H_3 = 1.8$  km, which is close to the value (1.6 km) for the tropical model atmosphere (see Table 1).

The AFCRL spectroscopic line parameters<sup>(12)</sup> for H<sub>2</sub>O have been tested against measurements at John Hopkins<sup>(14, 15)</sup> of absorption along

6 passes through a 100 ft long tube containing water vapor and nitrogen. Figures 20 and 21 compare our transmission calculations with the laboratory data. The agreement is quite good in the 20 - 25  $\mu\text{m}$  case, shown in Figure 20. Over this spectral range the average transmission was measured to be 59%, while the calculation yielded 57%.

In the 15 - 20  $\mu\text{m}$  spectral region the calculated transmission is generally (25 - 50%) higher than measured, as seen in Figure 21. The lines fit fairly well, except that the resolution chosen for the computed spectrum ( $1 \text{ cm}^{-1}$  half width at half maximum) is a bit high. We infer that the water vapor continuum is stronger here than we calculate from the data of Refs. 4 and 13.

The mole fraction of water vapor is 0.0027 (vs  $\alpha = .02$  to  $.04$ ) in the case shown in Figure 20, while  $\chi = 0.04$  (vs  $\alpha = .007$  to  $.028$ ) for that shown in Figure 21. Thus the absorption coefficient is proportional to the total concentration in the first case, and proportional to the  $\text{H}_2\text{O}$  concentration in the second.

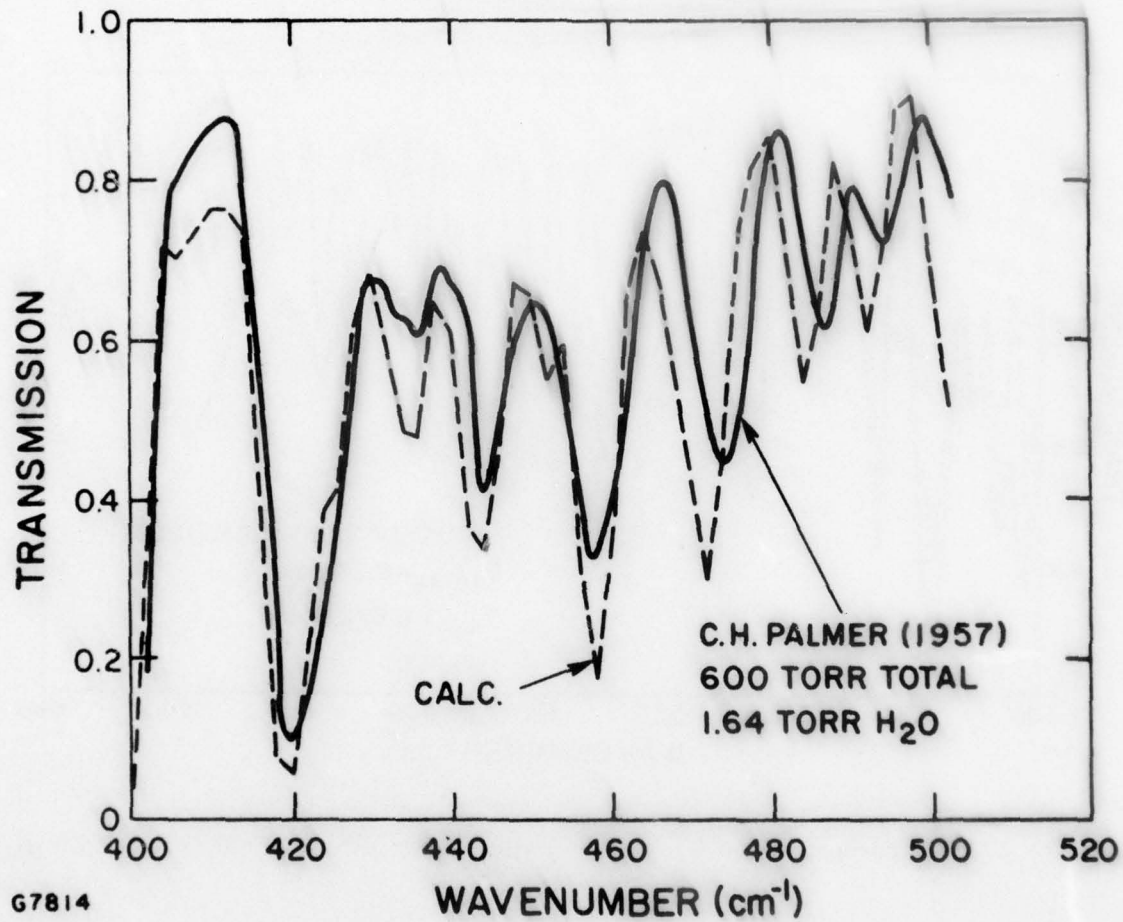


Figure 20. Transmission by Water Vapor Over 600 ft Path (20-25  $\mu$ )

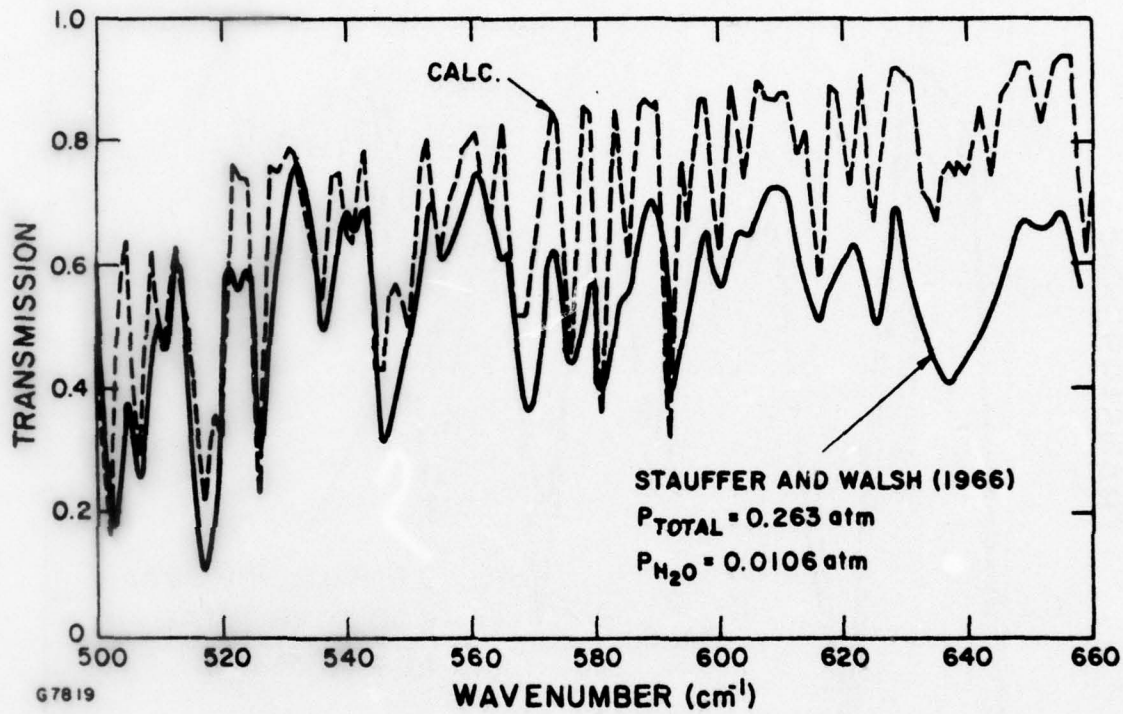


Figure 21. Transmission by Water Vapor Over 600 ft Path (15.2 - 20  $\mu$ )

## 5.2 TRANSMISSION IN 16-21 $\mu\text{m}$ WINDOW

Figure 22 shows the calculated transmission for a vertical line of sight originating at the altitude of AMOS. The amount of water vapor overhead is  $1 \text{ gm/cm}^2$ . Figures 9 and 10 indicate that this humid condition is encountered occasionally in the Hawaiian Islands.

The major absorber is seen to be the  $\text{H}_2\text{O}$  continuum ( $\bar{t} = 30\%$ ). The structure in the spectrum is due to  $\text{H}_2\text{O}$  lines, whose transmission averaged over this region is 40%.  $\text{CO}_2$  also absorbs in the 16.5-17.5  $\mu\text{m}$  region. Ozone absorption is negligible at these wavelengths.

The transmission by the individual absorbing components has been averaged over the 16.5-20.8  $\mu\text{m}$  region and displayed in Figures 23 to 26 for seven cases. For the water vapor lines we have very nearly  $-\ln t \propto u^{1/2}$ , as shown in Figure 23. This behavior is typical of strong line absorption. Indeed, our line-by-line results show that strong lines ( $\bar{x} \geq 3$ ) contribute 80% of the average equivalent line width,  $\bar{W}$ , even for the smallest value of  $u$  considered.

Individual cases for the water vapor continuum calculations are shown as data points in Figure 23. In these cases the total gas concentration,  $n_t$ , is constant, but  $\chi$ ,  $n_l$  and  $u = \chi n_l$  are variable. The mole fraction of water is generally small compared with  $\alpha$ , the total-concentration coefficient appearing in Eqs. (38) and (39). We thus would expect Eq. (49) to determine the transmission. Accordingly  $-\ln t$  should scale linearly with  $u$ . Our individual cases fit this expectation closely; there is a little scatter in Figure 23 because the condition  $\chi \ll \alpha$  is not perfectly fulfilled in every case.



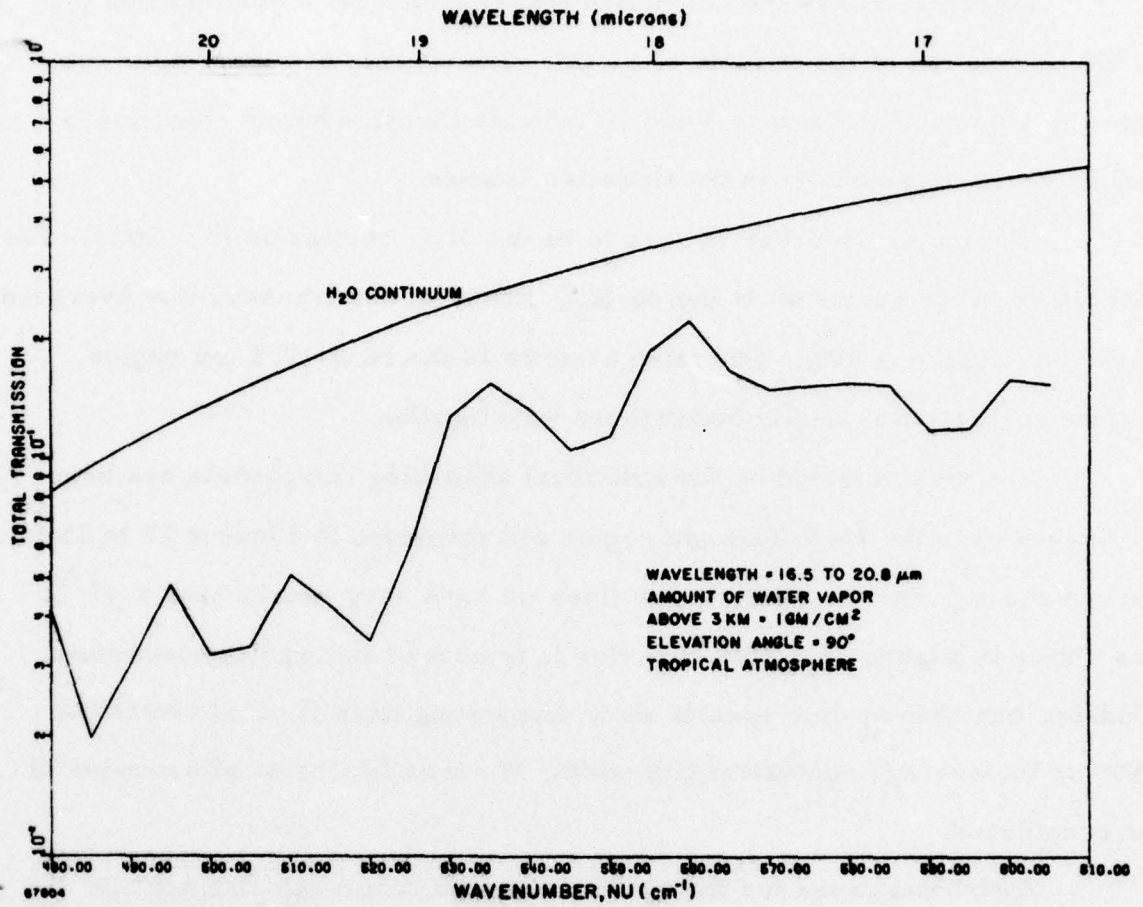
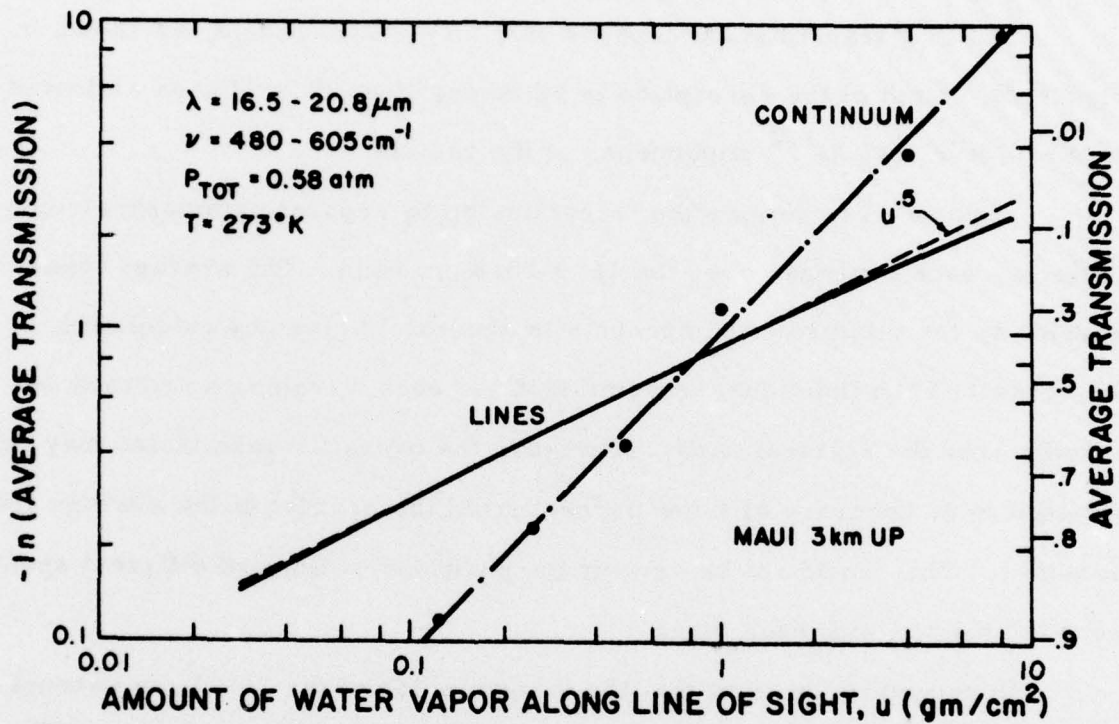


Figure 22. Transmission Through a Humid Tropical Atmosphere



G7818

Figure 23. Transmission by  $\text{H}_2\text{O}$  Lines and Continuum in 16-21  $\mu$  Window vs  $u$

Maps of water vapor transmission versus elevation angle and amount of water vapor overhead appear in Figures 24 and 25. Since the transmission depends only on  $u$ , the constant transmission lines shown have the form

$$u = u_1 \csc \theta = \text{const.}$$

The  $\text{CO}_2$  transmission depends only on elevation angle, as shown in Figure 26. Most of the absorption is by strong lines ( $\tilde{\nu} \gtrsim 10$ ), as indicated by the  $-\ln t \propto (\csc \theta)^{1/2}$  dependence of the results.

Figures 23 to 26 give the transmission by separate atmospheric constituents, each averaged over the 16.5-20.8  $\mu\text{m}$  band. The average transmission by the mixture of components is accurately given by calculating the product of the individual transmissions at each wavelength and then averaging over the spectral band. However, the overall transmission may be obtained to an accuracy of a few percent from the product of the average transmissions. This would not be valid if the positions of lines of different species were correlated with each other.

In summary, we find that the transmission of the 16-21  $\mu\text{m}$  channel is poor ( $\lesssim 60\%$ ) for viewing extra-atmospheric sources from AMOS, unless we look at high elevation angles under unusually dry conditions.

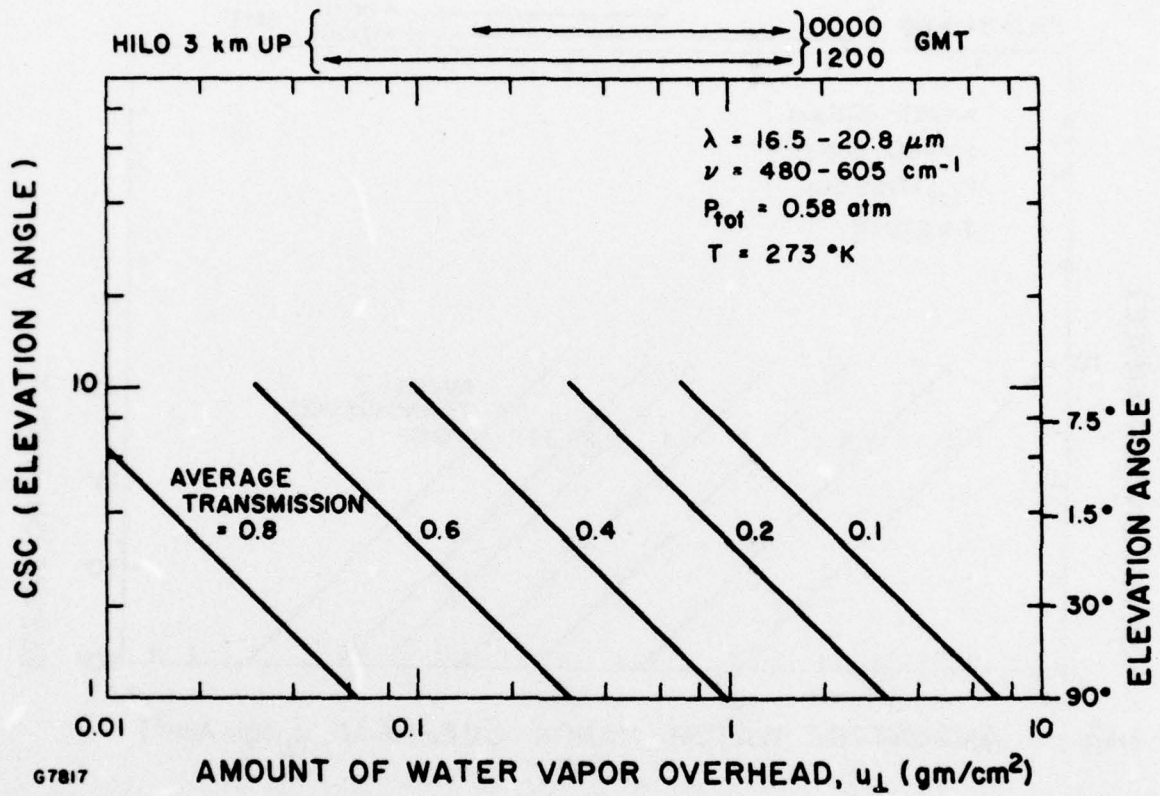


Figure 24. Map of Transmission by H<sub>2</sub>O Lines in 16-21  $\mu\text{m}$  Band

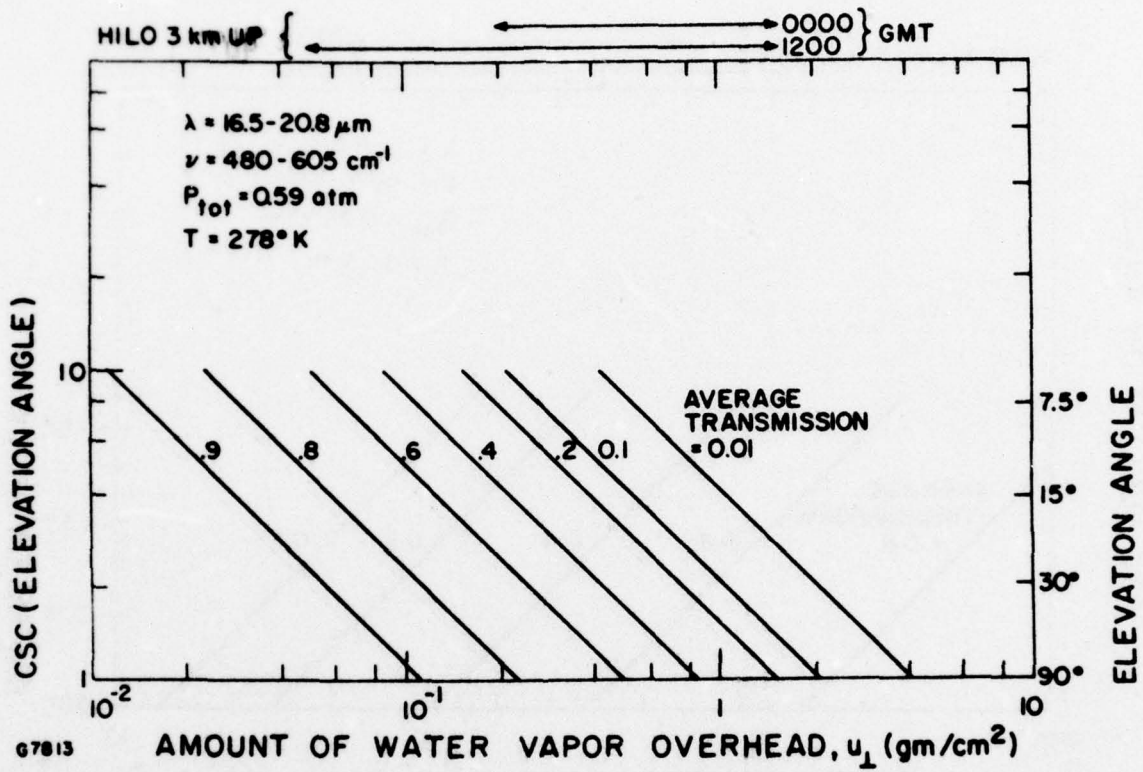
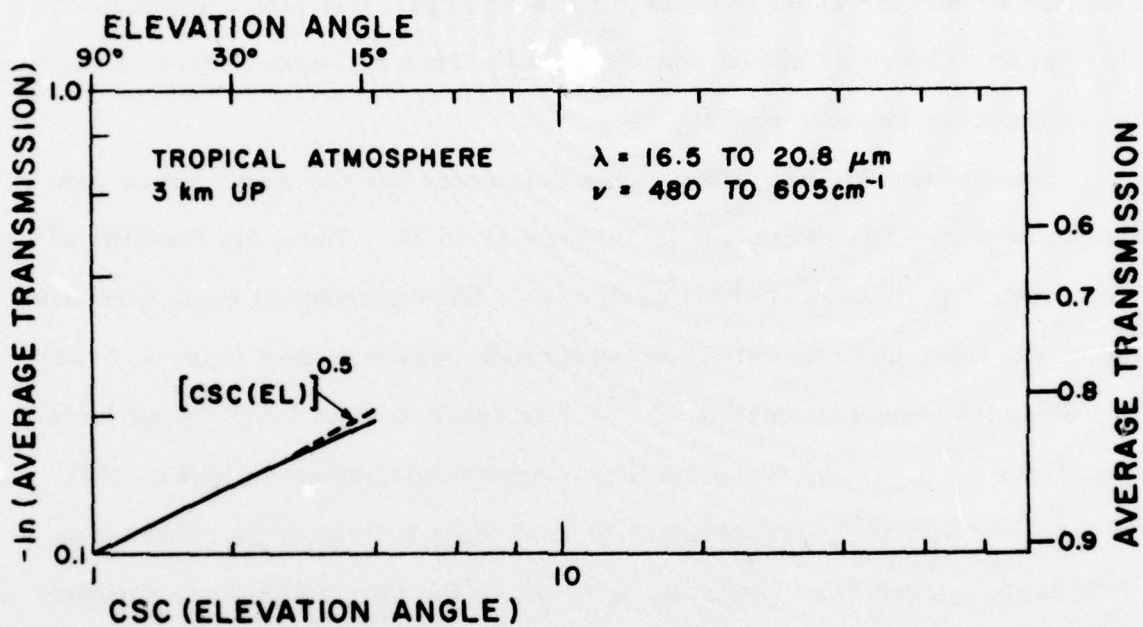


Figure 25. Map of Transmission by H<sub>2</sub>O Continuum in 16-21 μm Band



67815

Figure 26. Transmission by CO<sub>2</sub> Lines vs Elevation Angle in 16-21 μm Band

### 5.3 TRANSMISSION IN THE 8-13 $\mu\text{m}$ WINDOW

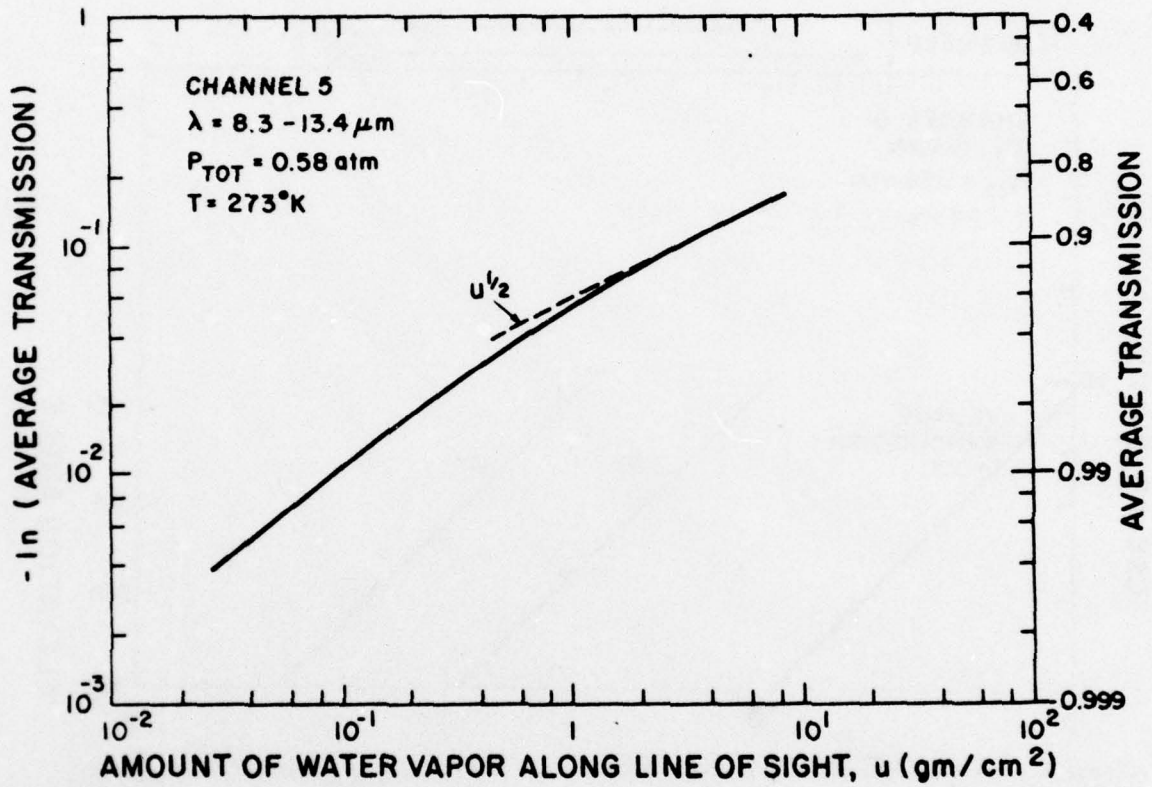
The 8-13  $\mu\text{m}$  region is much more favorable for infrared observations through the atmosphere. Water vapor lines are relatively transparent, as seen in Figures 27 and 28. The significant absorbing lines are strong, as shown by the  $-\ln t \propto u^{1/2}$  dependence in Figure 27, but they are widely separated so that the average transmission is high. For small amounts of water vapor, Figure 27 shows some deviation from the square-root relationship as the lines become weaker.

Our results for individual cases calculated for the water vapor continuum are shown as data points in Figures 29 to 30. The mole fraction of water vapor,  $\chi$ , is indicated for each case. This quantity is to be compared with  $\alpha$ , the total-gas concentration coefficient, which ranges from  $\sim 0.001$  to  $0.004$  in this spectral region.<sup>(4, 13)</sup> For small  $u$  (and small  $\chi$ ) we have generally  $\chi \ll \alpha$ , so the transmission is approximately given by Eq. (49) and  $-\ln t$  is reasonably proportional to  $u$  as seen in Figure 29. For large  $u$  (and large  $\chi$ ), we have generally  $\chi \gg \alpha$ , so the transmission is approximately given by Eq. (48) and  $-\ln t$  is proportional to  $u^2/\ell$  as seen in Figure 30.

These two regimes are displayed on the map of continuum transmission (Figure 31). For small  $\chi$ , lines of constant transmission are given, as in Figure 25, by the relation  $u = u_{\perp} \csc \theta = \text{const.}$  For large  $\chi$ , lines of constant transmission are given by  $u^2/\tilde{\ell} = \text{const.}$  Since  $\tilde{\ell}$ , defined by Eq. (47), is proportional to  $\csc \theta$ , constant transmission corresponds to the relation

$$u_{\perp}^2 \csc \theta = \text{const.}$$

in the  $\chi \gg \alpha$  regime. A more detailed analysis would produce curvature to the lines in Figure 31, with a smooth transition between regimes.



67820

Figure 27. Transmission by  $\text{H}_2\text{O}$  Lines in 8-13  $\mu\text{m}$  Band vs  $u$



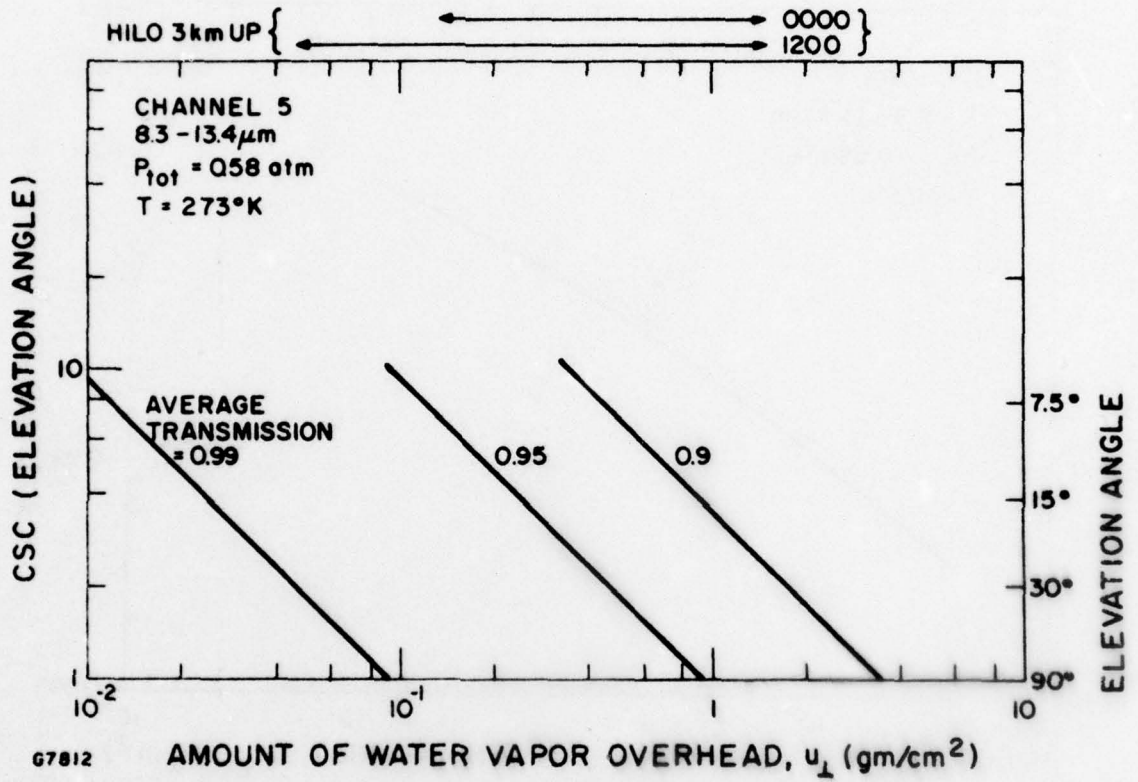


Figure 28. Map of Transmission by H<sub>2</sub>O Lines in 8-13  $\mu\text{m}$  Band

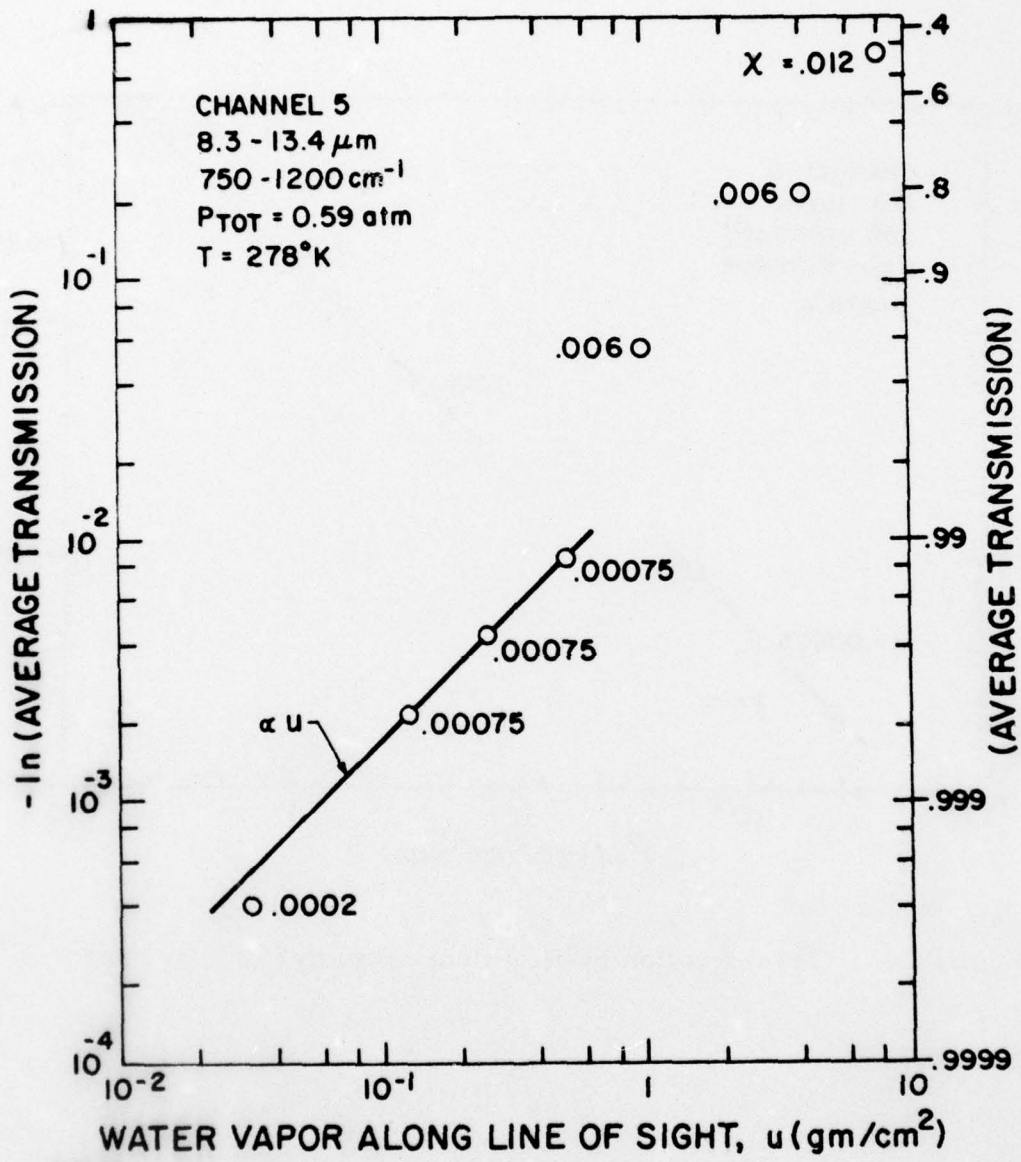
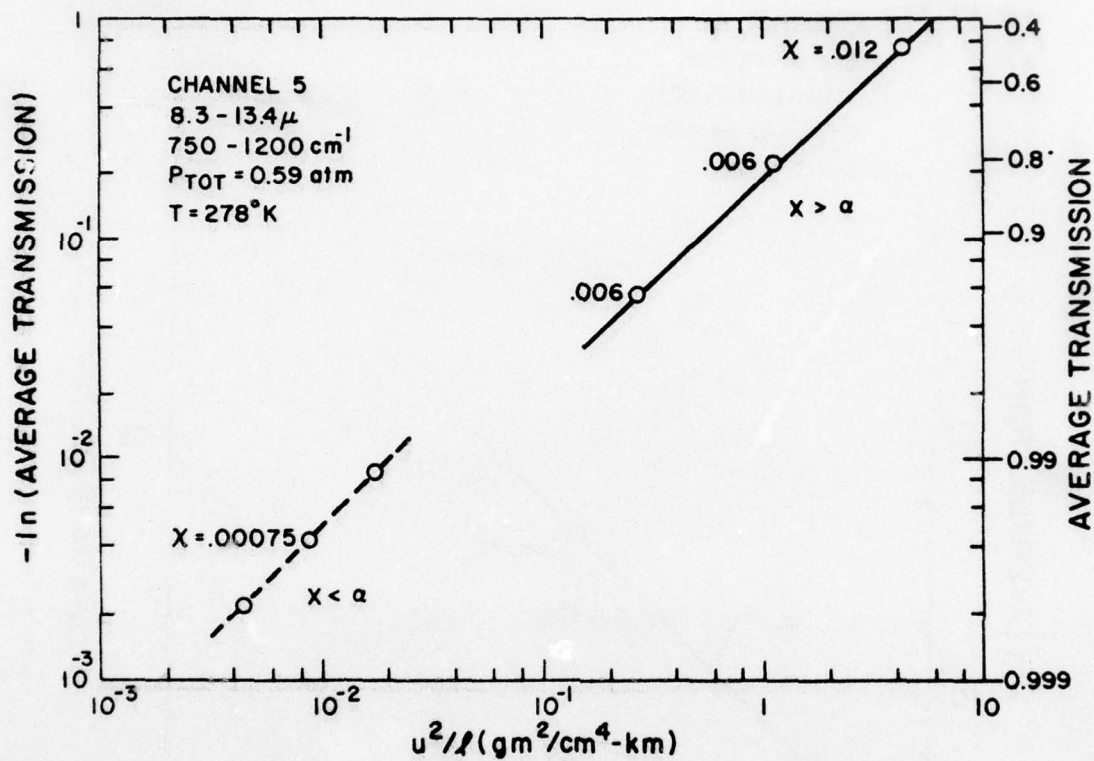


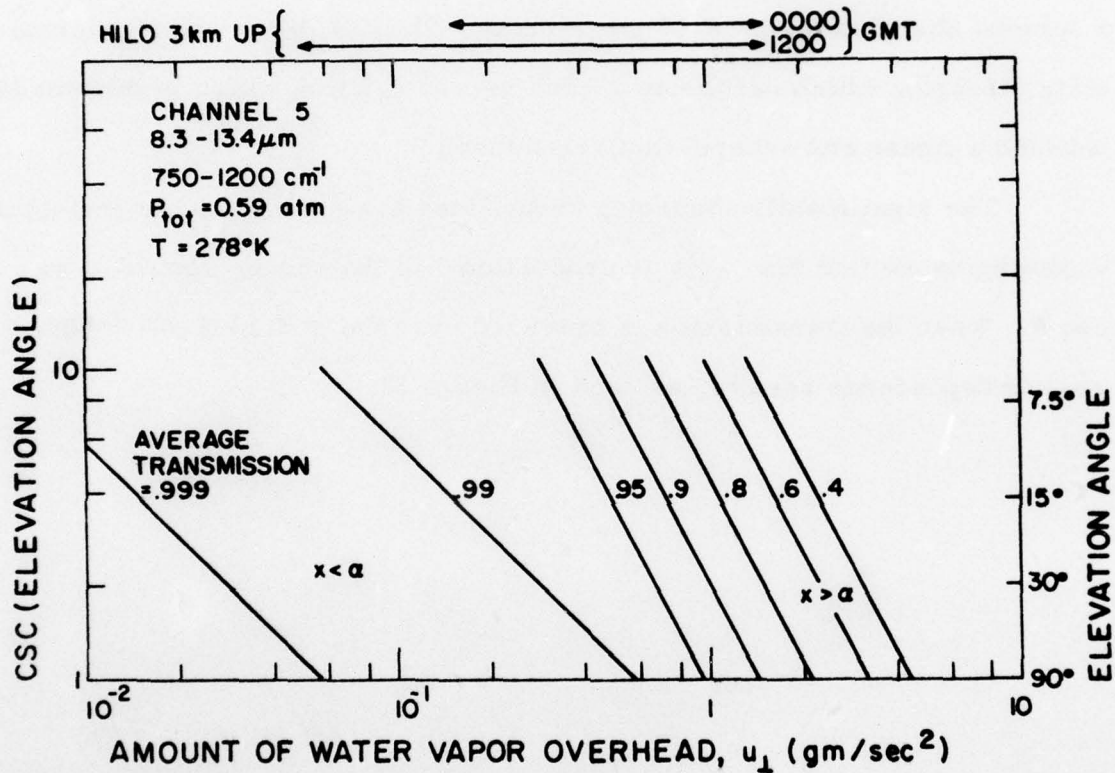
Figure 29. Transmission by  $\text{H}_2\text{O}$  Continuum in 8-13  $\mu\text{m}$  Band vs  $u$



.00020

G7821

Figure 30. Transmission by  $\text{H}_2\text{O}$  Continuum in 8-13  $\mu\text{m}$  Band vs  $u^2/l$



67811

Figure 31. Map of Transmission by  $\text{H}_2\text{O}$  Continuum in the 8-13  $\mu\text{m}$  Band

In general, absorption by water vapor in the 8-13  $\mu\text{m}$  window is small under dry conditions, but is significant and varies rapidly with amounts of water vapor under humid conditions.

The effects of  $\text{CO}_2$  and  $\text{O}_3$  are presented in Figure 32. Neither is a serious absorber in the 8-13  $\mu\text{m}$  window. The  $\text{CO}_2$  lines are of intermediate strength, which results in a  $-\ln t$  vs  $\text{csc } \theta$  curve which is intermediate between a linear and square-root relationship.

The significantly absorbing ozone lines are strong, and at individual wavelengths we find that  $-\ln t$  is proportional to the square root of  $u$  or  $\text{csc } \theta$ . When the transmission is averaged over the 8.3-13.4  $\mu\text{m}$  range, a weaker dependence results, as seen in Figure 32.

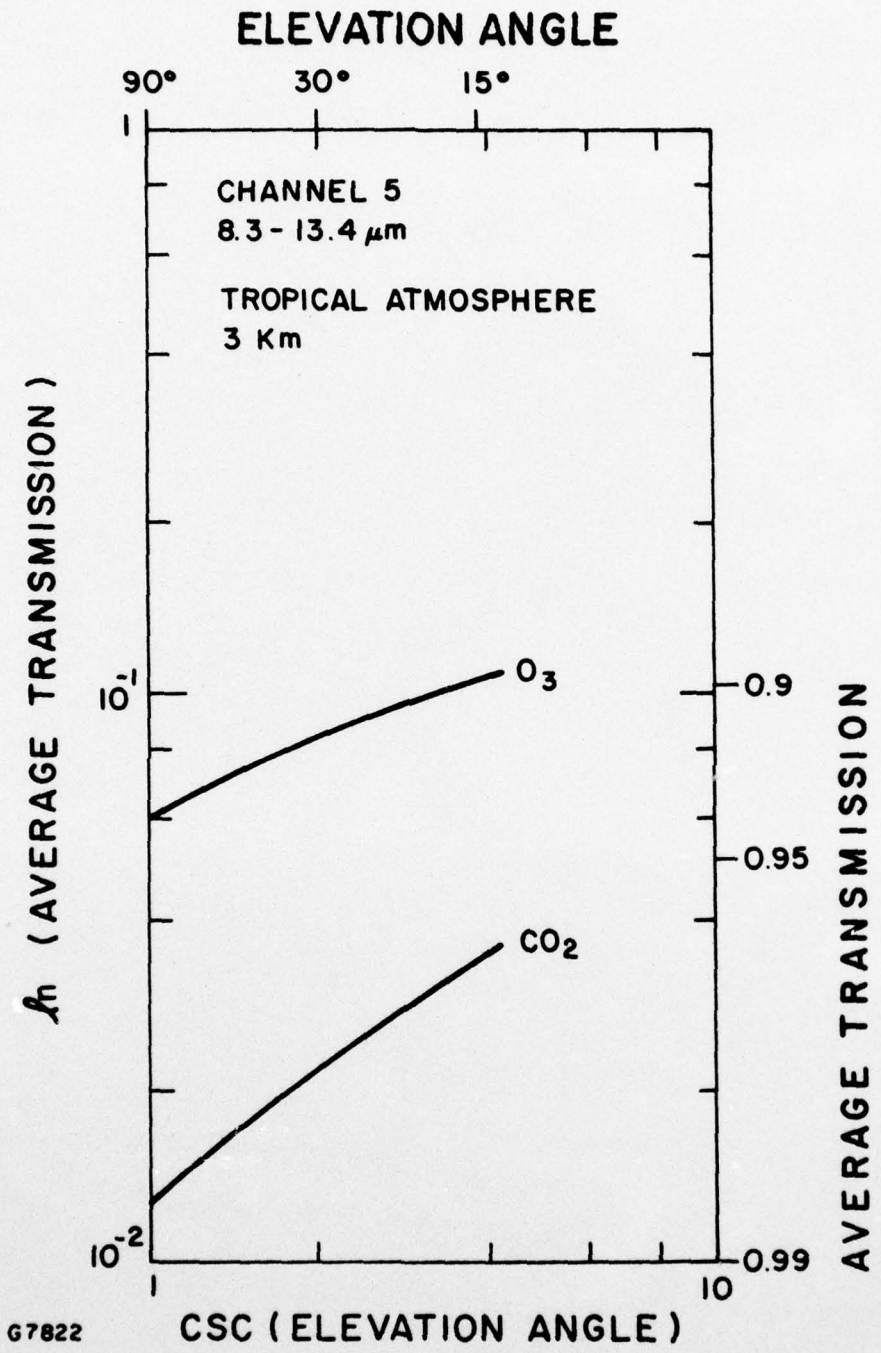


Figure 32. Transmission by CO<sub>2</sub> and O<sub>3</sub> in the 8-13  $\mu\text{m}$  Band

## 6.0 CONCLUSIONS

In this section we will present our transmission predictions for the Hawaiian atmosphere above 3 km in summary form, and compare them with the alternate results.

In the previous section, the transmission was given for individual atmospheric constituents -  $H_2O$ ,  $CO_2$  and  $O_3$  lines, as well as the  $H_2O$  continuum. For any amount of water vapor and zenith angle, the overall transmission may be obtained by multiplication.

Typical results for our detailed calculations of the overall transmission are shown by the solid lines in Figures 33 and 34. The lower solid curves are for  $u_{\perp} = 0.125 \text{ gm/cm}^2$  of water vapor overhead, a "dry" condition occasionally encountered at night (see Figure 10). The upper solid curves are for  $u_{\perp} = 1 \text{ gm/cm}^2$  of water vapor overhead. This humid condition is sometimes found day or night, as seen in Figures 9 and 10.

The slopes of these curves range from  $n = 0.56$  to  $0.74$ , where  $n$  is the exponent in the expression

$$t = \exp - a (\csc \theta)^n. \quad (71)$$

Figures 33 and 34 also show the average transmission in channels 5 and 6 calculated using the LOWTRAN 3 code<sup>16, 17</sup> for the AFCRL tropical model atmosphere (dash-dot lines). As shown on Figures 9 and 10, this model entails  $u_{\perp} = 0.8 \text{ gm/cm}^2$  of water vapor above 3 km altitude. The LOWTRAN transmission predictions, relative to our more detailed

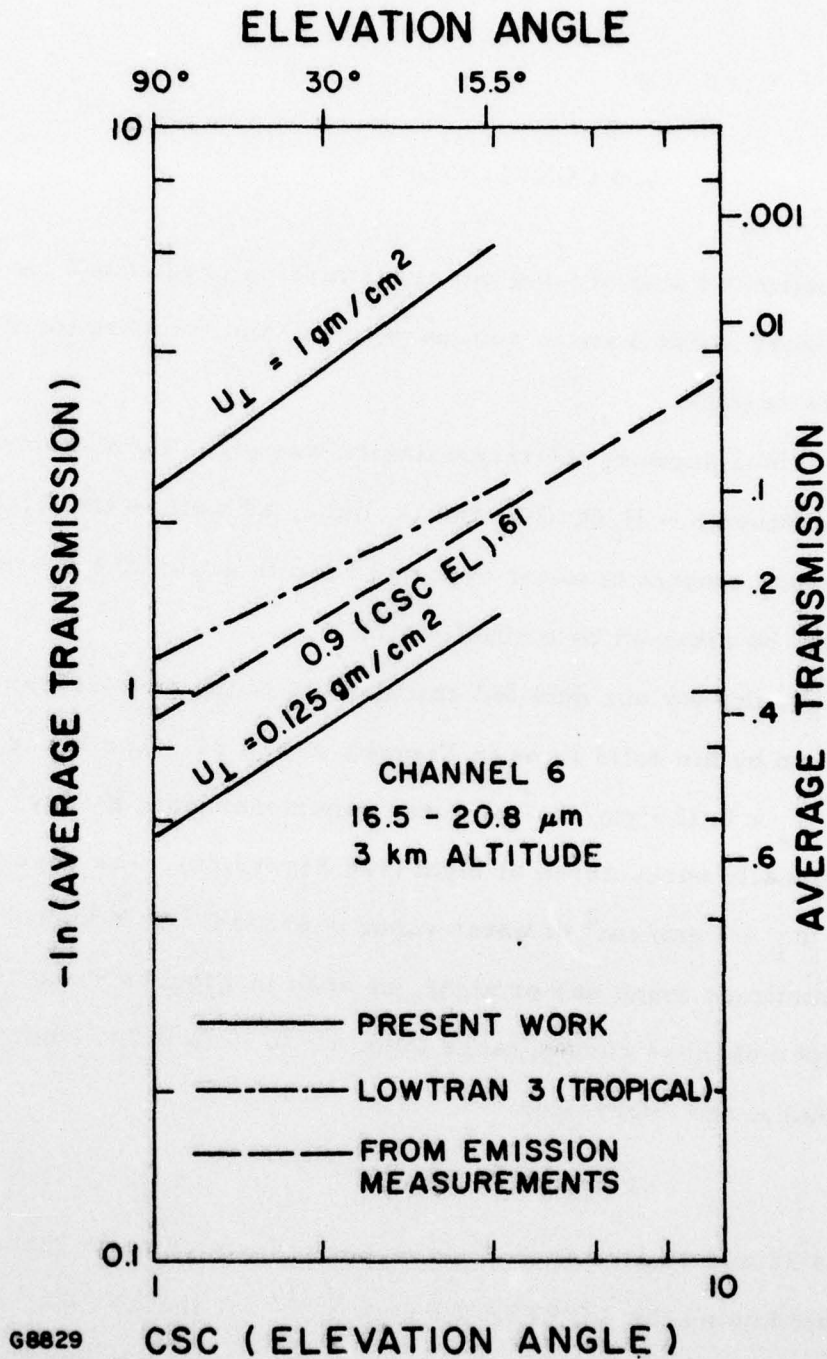


Figure 33. Predicted Transmission from 3 km to Outer Space vs Elevation Angle. Present results for large ( $1 \text{ gm/cm}^2$ ) and small ( $0.125 \text{ gm/cm}^2$ ) amounts of water vapor overhead are compared with LOWTRAN calculations and predictions based upon a measurement of atmospheric radiance.



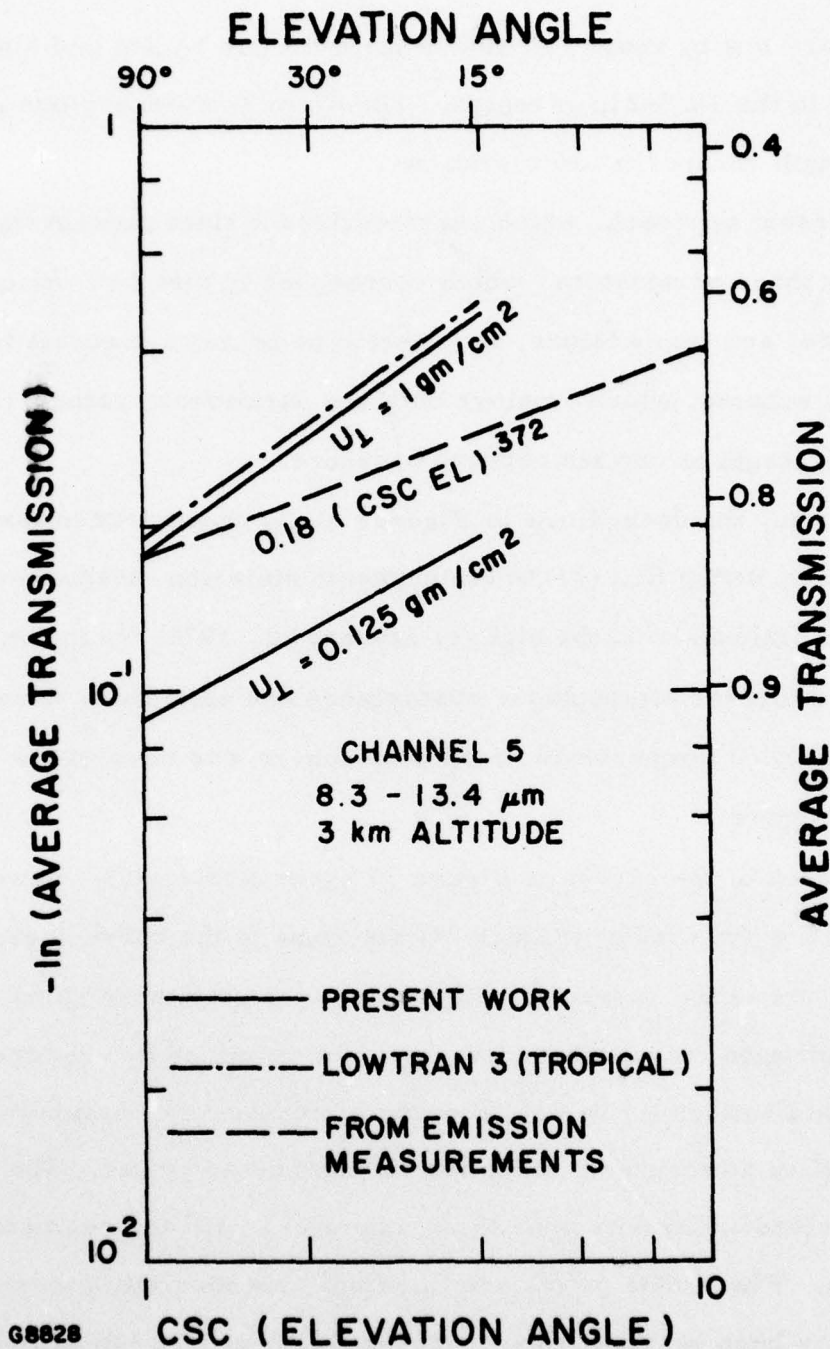


Figure 34. Predicted Transmission from 3 km to Outer Space vs Elevation Angle. Present results for large (1 gm/cm<sup>2</sup>) and small (0.125 gm/cm<sup>2</sup>) amounts of water vapor overhead are compared with LOWTRAN calculations and predictions based upon a measurement of atmospheric radiance.

calculations, are low by about 3 to 10% in the 8-13  $\mu\text{m}$  region and high by factors of 2 to 16 in the 16.5-21 $\mu\text{m}$  region. The error is most serious in the longer wavelength channel at low elevations.

The present approach, which characterizes a slant path through the atmosphere by three parameters, which correspond to effective optical depth, pressure, and temperature, is expected to be more accurate than the LOWTRAN scheme, which employs only one parameter, namely the equivalent path length at one atmosphere pressure.

In addition, the dashed line in Figures 33-34 shows transmission values derived by fitting Eq. (71) to atmospheric emission measurements<sup>18</sup> made from Mt. Haleakala on the night of January 22, 1976. In this analysis it was assumed that the atmospheric absorptance and emissivity were equal, and that the effective temperature of the atmosphere was equal to the local ambient temperature.

The slopes of the curves in Figure 33 agree fairly well. However for the 8.3 - 13.4  $\mu\text{m}$  window (Figure 34) the slope of the curve based on emission measurements is seen to be much less than for those based on molecular absorption calculations. We have not explained this discrepancy.

To obtain emissivity values from the atmospheric emission measurements an effective atmospheric temperature must be employed. The dependence of the derived emissivity upon the temperature used is presented in Figures 35-36. Where data points are missing, an emissivity greater than unity would have been required to account for the measured intensities.

For an elevation angle of  $90^\circ$  the spectral sky radiance was measured to be  $1.6 \times 10^{-6}$  watts/cm<sup>2</sup>-sr-cm<sup>-1</sup> in channel 5 and  $7.8 \times 10^{-6}$  watts/cm<sup>2</sup>-sr-cm<sup>-1</sup> in channel 6. We have already presented predictions of sky

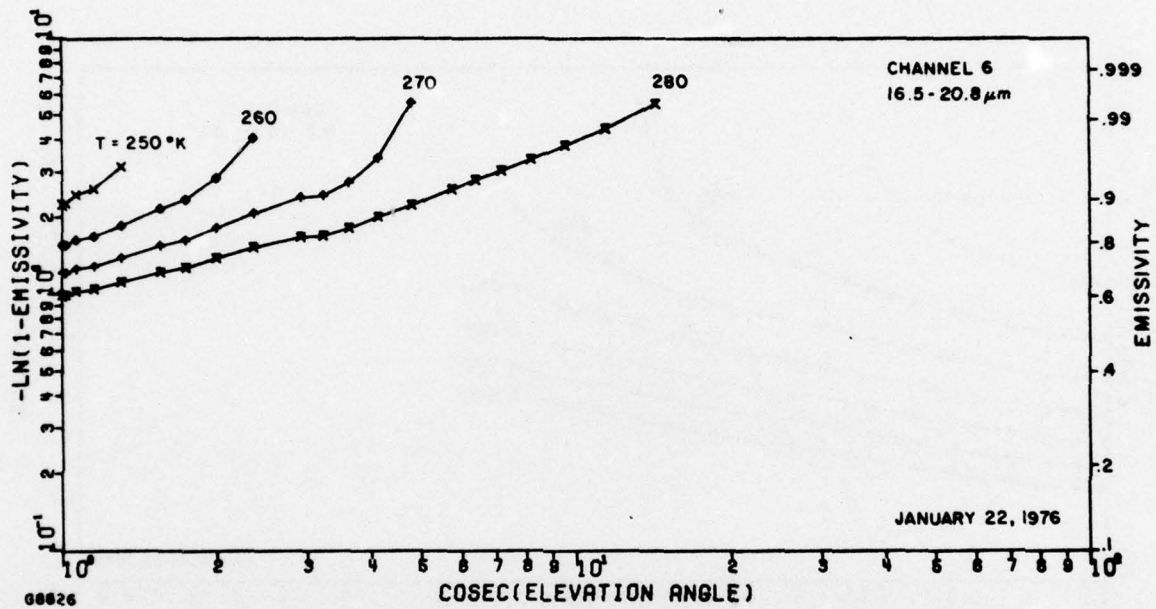


Figure 35. Emissivity of the Sky Measured by H. Kent at AMOS, for Various Assumed Atmospheric Temperatures

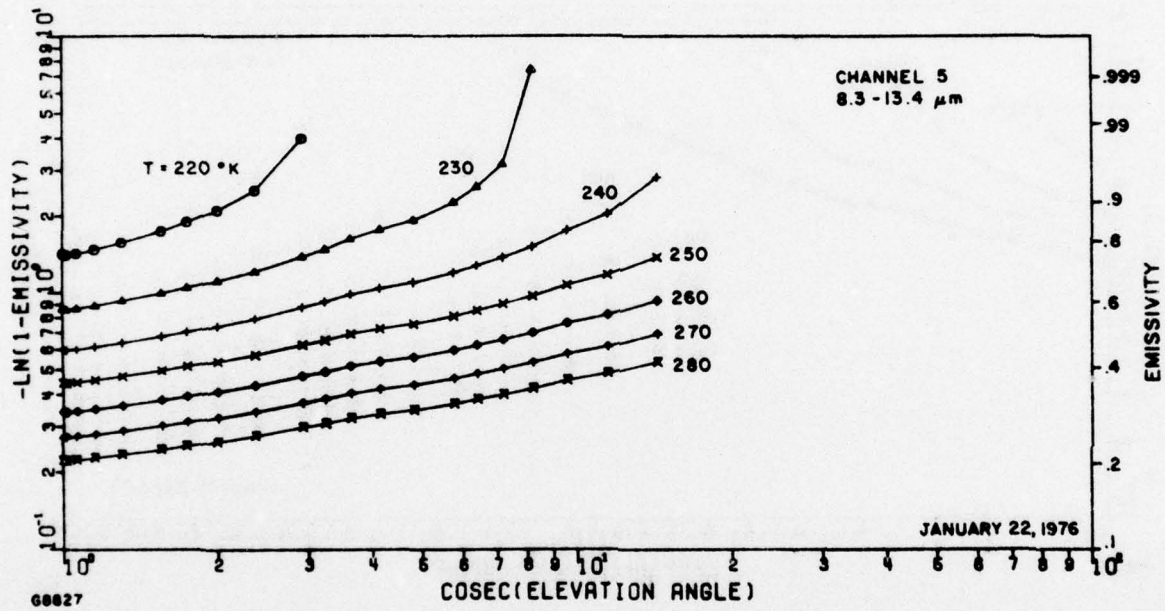


Figure 36. Emissivity of the Sky Measured by H. Kent at AMOS, for Various Assumed Atmospheric Temperatures

radiance in channel 6 due to H<sub>2</sub>O lines for real atmospheric conditions in Figure 19. The maximum predicted value is about  $4.5 \times 10^{-6}$  watts/cm<sup>2</sup> - sr-cm<sup>-1</sup>. If we add the influence of the H<sub>2</sub>O continuum and CO<sub>2</sub> lines, we obtain a maximum of about  $6.8 \times 10^{-6}$  watts/cm<sup>2</sup> - sr-cm<sup>-1</sup>, which still lies below the measured data. The discrepancy is probably to be explained by additional sources of emission, such as cirrus clouds. A thin layer of cirrus could easily have an emissivity<sup>19</sup> of 0.2, or a spectral radiance at 230°K of  $1.4 \times 10^{-6}$  watts/cm<sup>2</sup> - sr-cm<sup>-1</sup>, which is sufficient to reconcile our calculations with the field measurements.

We conclude that real time measurements of sky emission have potential utility in determination of atmospheric transmission. The present study provides assistance in this procedure, especially in providing predictions of the effective temperature of the molecular emitters. However, we believe clouds may have a significant effect, which deserves further investigation. This study should include the effect of scattering, which reduces the transmission along a line of sight without a corresponding increase in emissivity.

\* \* \*

The basic conclusion of this work is that direct or indirect determination of the total amount of water vapor overhead is a prerequisite for the quantitative interpretation of infrared measurements through tropical atmospheres, even from an altitude of 3 km. The permissible elapsed time between the primary and secondary measurements is estimated as 1-2 hours; a more precise determination of the tolerance would be desirable. Records for 10 different nights at AMOS show the local absolute humidity changed by a factor of 2 or 3 within 20 to 40 minutes on three occasions.

ACKNOWLEDGMENT

The author is grateful to Mr. H. P. Kent and the AMOS staff for providing atmospheric radiance data.

## REFERENCES

1. Strong, J. and Plass, G. N., "The Effect of Pressure Broadening of Spectral Lines of Atmospheric Temperature," *Astrophys. J.* 112, 365-379 (1950).
2. Valley, S. L., ed., Handbook of Geophysics and Space Environments, AFCRL (1965).
3. McClatchey, R. A., et al., "Optical Properties of the Atmosphere," 3rd ed., AFCRL-72-0497 (24 August 1972).
4. Roberts, R. E., Selby, J. E. and Biberman, L. M., "Infrared Continuum Absorption by Atmospheric Water Vapor in the 8-12  $\mu\text{m}$  Window," *Appl. Opt.* 15, 2085-2090 (1976).
5. Lindquist, G. H. and Simmons, F. S., "A Band Model Formulation for Very Nonuniform Paths," *J. Quant. Spectry. Radiat. Transfer* 12, 807-820 (1972).
6. Riehl, H., Tropical Meteorology (McGraw-Hill, New York, 1954).
7. Malkus, J. S. and Riehl, H., Cloud Structure and Distributions Over the Tropical Pacific Ocean (University of California Press, Berkely, 1964).
8. Brousaides, F. J., "The Radiosonde Hygristor and Low Relative Humidity Measurements," *Bull. Am. Meteorol. Soc.* 56, 229-233 (1975).
9. Miller, J. M., ed., "Geophysical Monitoring for Climatic Change/ No. 3/Summary Report - 1974," NOAA/ERL (August 1975).
10. Mendonca, B. G., "Local Wind Circulation on the Slopes of Mauna Loa," *J. Appl. Meteorol.* 8, 533-541 (1969).
11. Mendonca, B. G. and Iwaoka, W. T., "The Trade Wind Inversion at the Slopes of Mauna Loa, Hawaii," *J. Appl. Meteorol.* 8, 213-219 (1969).
12. McClatchey, R. A., et al., "AFCRL Atmospheric Absorption Line Parameters Compilation," AFCRL-TR-73-0096 (26 January 1973).
13. Burch, D. E., Gryvnak, D. A. and Gates, F. J., "Continuum Absorption by  $\text{H}_2\text{O}$  between 330 and 825  $\text{cm}^{-1}$ ," AFCRL-TR-74-0377/Philco-Ford U-6095 (September, 1974).

14. Palmer, C.H., "Long Path Water Vapor Spectra with Pressure Broadening, I.  $20\mu$  to  $31.7\mu$ ," J. Opt. Soc. Am. 47, 1024-1028 (1957).
15. Stauffer, F.R. and Walsh, T.E., "Transmittance of Water Vapor - 14 to 20 Microns," J. Opt. Soc. Am. 56, 401-405 (1966).
16. McClatchey, R.A., et al., "Optical Properties of the Atmosphere", 3rd ed., AFCRL-72-0497 (24 August 1972).
17. Selby, J.E.A., and McClatchey, R.A., "Atmospheric Transmittance from 0.25 to  $28.5\mu\text{m}$ : Computer Code LOWTRAN 2", AFCRL-72-0745 (29 December 1972).
18. Kent, H.P., "IR Atmospheric Measurements", AERL, Interim Technical Report for 30 June 1975-28 February 1976, Contract F30602-75-C-0235.
19. Fleming, J.R., and Cox, S.K., "Radiative Effects of Cirrus Clouds", J. Atmos. Sci. 31, 2182-2188 (1974).

END  
11-77